Genetic and physical interactions reveal overlapping and distinct contributions to meiotic double-strand break formation in *C. elegans*

Marilina Raices[1], Fabiola Balmir[1], Nicola Silva[3] , Wei Li[1,2], , McKenzie K. Grundy[4], Dane K. Hoffman[1,$], Elisabeth Altendorfer[5], Carlos Jaime Camacho[6],Kara A. Bernstein[4,7], Monica P. Colaiácovo[5] and Judith Yanowitz[1,8,*]

[1]Magee-Womens Research Institute, Pittsburgh, PA 15213 USA; [2]Tsinghua U. Medical School, China; [3]Department of Biology, Masaryk University, Czech Republic; [4]Department of Microbiology and Molecular Genetics, University of Pittsburgh School of Medicine, UPMC Hillman Cancer Center, Pittsburgh, Pennsylvania; [5]Department of Genetics, Blavatnik Institute, Harvard Medical School, 77 Avenue Louis Pasteur, Room 334, Boston, MA 02115, USA; [6]Department of Computational and Systems Biology, University of Pittsburgh School of Medicine, Pittsburgh, PA, 15213 USA; [7]Department of Biochemistry and Biophysics, University of Pennsylvania, Penn Center for Genome Integrity, Philadelphia, Pennsylvania; [8]Department of Obstetrics, Gynecology and Reproductive Sciences, University of Pittsburgh School of Medicine, Pittsburgh, PA, 15213 USA.

[$]Current address: Lester & Sue Smith Breast Center, Department of Molecular & Cellular Biology, Baylor College of Medicine, Houston, TX 77030.

***Corresponding author:** yanowitzjl@mwri.magee.edu

Running title: DSB complexes in *C. elegans*

Keywords: meiosis, double-strand break, *C. elegans*, SPO11, Crossover

ABSTRACT

Double-strand breaks (DSBs) are the most deleterious lesions experienced by our genome. Yet, DSBs are intentionally induced during gamete formation to promote the exchange of genetic material between homologous chromosomes. While the conserved topoisomerase-like enzyme Spo11 catalyzes DSBs, additional regulatory proteins—referred to as "Spo11 accessory factors"— regulate the number, timing, and placement of DSBs during early meiotic prophase ensuring that SPO11 does not wreak havoc on the genome. Despite the importance of the accessory factors, they are poorly conserved at the sequence level suggesting that these factors may adopt unique functions in different species. In this work, we present a detailed analysis of the genetic and physical interactions between the DSB factors in the nematode *Caenorhabditis elegans* providing new insights into conserved and novel functions of these proteins. This work shows that HIM-5 is the determinant of X-chromosome-specific crossovers and that its retention in the nucleus is dependent on DSB-1, the sole accessory factor that interacts with SPO-11. We further provide evidence that HIM-5 coordinates the actions of the different accessory factors sub-groups, providing insights into how components on the DNA loops may interact with the chromosome axis.

INTRODUCTION

One of the seminal events during meiosis is the formation of crossovers (CO) during the first meiotic division. While COs create new combinations of alleles through the exchange of genetic material between homologs, they also establish physical connections that ensure their proper alignment on the meiotic spindle and their subsequent segregation to opposite ends of the spindle. In the absence of COs, homologs segregate randomly, leading to gametes with altered chromosome numbers and subsequent fetal aneuploidies. In humans, aneuploidy is

observed in 1 of 160 live births (Dungan, 2002) and in >50% of miscarriages (Hassold et al., 2007) underscoring the importance of proper CO formation.

A necessary early step in CO formation is the creation of DNA double-strand breaks (DSBs) catalyzed by the widely conserved Spo11 enzyme (Bergerat et al., 1997; Keeney et al., 1997). Although Spo11 is essential for DSB formation, it does not function alone: additional proteins regulate the timing, placement, and number of DSBs (Cole et al., 2010; Hinman et al., 2021; Keeney, 2008). In *Saccharomyces cerevisiae*, where DSB formation has been best characterized, at least nine other proteins interact with Spo11 to regulate its recruitment and activation (Lam & Keeney, 2015; Martini et al., 2006). *In vivo* and *in vitro* physical interaction studies have revealed that these proteins form several subcomplexes. Briefly, the RMM complex (Rec114, Mer2, and Mei4) is loaded on chromosomes early in prophase and is required for Spo11 binding to sites of DNA cleavage (J. Li et al., 2006; Sasanuma et al., 2007). Activation of Mer2 requires phosphorylation by cyclin-dependent kinase (CDK) (Henderson et al., 2006), suggesting that Mer2 links DSB formation to the progression of the meiotic program (Arora et al., 2004; Henderson et al., 2006; J. Li et al., 2006; Maleki et al., 2007). Rec102 and Rec104 form another subcomplex that facilitates Spo11 dimerization and its association with DSB sites (Arora et al., 2004; Kee & Keeney, 2002; Prieler et al., 2005; Sasanuma et al., 2007). Ski8 binds Spo11 and is important for Spo11 nuclear localization (Arora et al., 2004). Finally, the Mre11–Rad50–Xrs2 (MRX) complex is also required for DSB formation but requires all the other DSB proteins to associate with DSB sites. Despite their importance, most of these proteins are poorly conserved at the amino acid level although homologs have been identified for several of these in organisms ranging from plants to worms to mice (Cole et al., 2010; Kumar et al., 2010). While a recent study of plants has presented a similar model for DSB induction as in yeast (Vrielynck et al., 2021), our understanding of the DSB machinery in metazoans is lacking.

72 *In vitro* biochemical studies have shown that *C. elegans* SPO-11 is monomeric and, even when
73 it is able to bind dsDNA, it does not exhibit DNA cleavage activity (Yeh et al., 2017). This
74 observation strongly supports the hypothesis that cofactors are needed for DSB induction.
75 Indeed, *dsb-1*, *dsb-3*, *him-17*, *mre-11*, and *rad-50* are all essential for the introduction of breaks
76 in this organism (Chin & Villeneuve, 2001; Hayashi et al., 2007; Hinman et al., 2021; Reddy &
77 Villeneuve, 2004; Stamper et al., 2013). Other genes, including *xnd-1*, *him-5, rec-1, dsb-2,*
78 *cep-1,* and *parg-1* have more limited roles in break induction, with the former two genes
79 required to ensure the full complement of DSBs on the X chromosome (Janisiw et al., 2020;
80 Meneely et al., 2012; Rosu et al., 2013). *xnd-1* is also unique among the accessory factors in
81 influencing the timing of DSBs; in the absence of *xnd-1*, there is precocious and rapid
82 accumulation of DSBs as monitored by the accumulation of the HR strand-exchange protein
83 RAD-51(Gao et al., 2015; McClendon et al., 2016; Wagner et al., 2010). CO positioning is
84 altered in all situations where DSB levels are affected, but the *rec-1* mutation has a profound
85 effect on the distribution of meiotic COs (Rose & Baillie, 1979) with only a minor reduction in
86 total DSB numbers (Chung et al., 2015).

87 Prior analysis of *rec-1* and *him-5* found these genes to be paralogs that function cooperatively
88 to ensure wild-type DSB levels (Chung et al., 2015). *him-5* has also been shown to have
89 synthetic interactions with *cep-1,* and epistatic relationships with *xnd-1* and *him-17*, in part
90 because *xnd-1* regulates *him-5* transcriptionally (McClendon et al., 2016). These studies also
91 revealed roles for *him-5* in coordinating DSB induction with downstream repair.

92 In this study, we expand the analysis of the genetic interactions between the SPO-11
93 accessory factors in *C. elegans* and provide the first biochemical studies of protein-protein
94 interactions between these factors by co-immunoprecipitation and support of yeast-two hybrid
95 (Y2H). We propose for the first time a possible complex that regulates DSB formation in *C.*
96 *elegans* and compare and contrast this to models recently proposed in yeast and plants

97 (Bouuaert et al., 2021, Vrielynck et al., 2021). Our results allow us to begin to elucidate the
98 regulatory events that control the localization, timing, and placement of meiotic DSBs in *C.*
99 *elegans*.

100

101 **RESULTS**

102 **HIM-5 is the essential factor for meiotic breaks in the X-chromosome**

103 Three of the DSB proteins appear to have a biased effect on X chromosome CO formation:
104 null alleles of *xnd-1* and *him-5* predominantly show a loss of CO intermediates on the X,
105 increases in univalent X chromosomes at diakinesis in half or almost all nuclei, respectively,
106 and an increase in XO male offspring resulting from nondisjunction of the X chromosome
107 during the meiotic division; the hypomorphic *him-17(e2806)* mutations shows increased
108 incidence of one unattached homolog pair in diakinesis and an increase in male production
109 consistent with an X-specific defect (Reddy & Villeneuve, 2004). To determine if these genes
110 function through a common underlying mechanism, we first performed yeast two-hybrid (Y2H)
111 assessing interactions with both high and low stringency. We observed a strong Y2H
112 interaction between XND-1 and HIM-17, and a weak one between HIM-17 and HIM-5 (Figure
113 1A). To validate these interactions, we also performed immunoprecipitations (IPs) of HIM-17
114 followed by mass spectrometry (MS). This identified XND-1, as well as 16 additional strong
115 interactors of HIM-17 (Figure 1B). Moreover, endogenous XND-1 was identified in western
116 blots of IPs performed independently using 3xHA-tagged HIM-17 epitopes, indicating a robust
117 interaction between these proteins (Figure 1C). In contrast, HIM-5 was not detected in either
118 the HIM-17 co-IPs or IP/MS, suggesting that the interaction observed by Y2H either exists very
119 transiently or was bridged by a protein expressed in yeast.

120

121 Prior studies from our group indicate that *xnd-1* regulates HIM-5 transcriptionally since ectopic
122 expression of *him-5::GFP* using the *pie-1* germline promoter, but not expression using the
123 endogenous *him-5* promoter, rescues the X chromosome nondisjunction defects conferred by
124 the *xnd-1* mutation (Wagner et al., 2010, Meneely et al., 2012; McClendon et al., 2016). Since
125 *xnd-1* and *him-17* both function to regulate X chromosome DSBs and their encoded proteins
126 physically associate (Figure 1A-C), we reasoned that *him-17* might also regulate *him-5*
127 expression. As seen in *xnd-1* mutants, ectopic expression of *Ppie-1::him-5* in *him-17* null
128 mutants rescued the X chromosome defects seen by the increase of XO male offspring from
129 XX hermaphrodites (known as the high incidence of males or "Him" phenotype) (34.98% of
130 males in *him-17(ok424)* vs. 7.02% in *pie1p::him-5;him-17(ok424)*) (Figure 1D). When *him-5*
131 was expressed from its own promoter (*Phim-5::him-5*), there was only a minor suppression of
132 both the Him phenotype and hatching rates (Figure 1D) and almost no change in univalent
133 formation (Figure S2) despite higher HIM-5 expression in the *Phim-5::him-5* strain than in the
134 *Ppie-1::him-5* strain (McClendon et al., 2016). Thus, we infer that XND-1 and HIM-17 both
135 regulate the expression of HIM-5 to promote X chromosome DSB/CO formation. In addition,
136 *xnd-1* and *him-17* have independent roles in DSB/CO formation since only null alleles of *him-*
137 *17*, but not *xnd-1* or *him-5*, confer a severe loss of DSBs (Meneely et al., 2012; Reddy &
138 Villeneuve, 2004; Wagner et al., 2010); and only *xnd-1* mutations affect the timing of
139 DSBs/repair (Wagner et al., 2010; McClendon et al., 2016).
140
141 We note that ectopic HIM-5 expression strongly rescued the embryonic lethality conferred by
142 the *him-17* null allele. While a small fraction of the lethality is attributed to X chromosome
143 nondisjunction, most results from missegregation of the autosomes. Thus, even though *him-5*
144 null mutant animals exhibit a profound loss of DSBs/COs on the X chromosomes with rare CO
145 defects on autosomes (Meneely et al., 2012), *him-5* expression can restore CO formation to
146 both autosomes and X chromosomes in the *him-17* mutant background. This strongly supports

147 a general role for HIM-5 in CO formation and further indicates that HIM-5 is sufficient to restore
148 COs on the X chromosome.
149
150 To further characterize the interaction between XND-1 and HIM-17, we also sought to
151 determine whether they colocalize on meiotic chromosomes using super-resolution
152 microscopy. Prior studies have shown that HIM-17 associates with meiotic chromatin (Reddy
153 & Villeneuve, 2004). Here we provide evidence that HIM-17 is preferentially enriched on the
154 autosomes, colocalizing with markers of active chromatin transcription. Co-staining the HIM-
155 17::HA transgenic line with anti-HA and anti-XND-1 antibodies showed that both proteins
156 predominantly localize off of the chromosome axes (marked with HTP-3), although some of
157 each protein can be seen close to the axes (Figure 1E and F).
158
159 **DSB-1 mediates interactions with SPO-11**
160 Since HIM-5 appears to be central to DSB/CO formation on the X chromosome and mutations
161 in *dsb-1* and *dsb-3* are required for all meiotic breaks, we next sought to determine whether
162 HIM-5 interacts with DSB-1, its paralog DSB-2, or DSB-3. We found that DSB-1 and DSB-2
163 show robust Y2H interactions and that DSB-1 and DSB-3 exhibit weak Y2H interactions
164 (Figure 2A), confirming results from a recent study (Hinman et al., 2021). We also found that
165 HIM-5 shows weak Y2H interactions with DSB-1 (Figure 2A). We confirmed the interaction
166 between DSB-1 and HIM-5 with co-IP, pulling down GFP::DSB-1 and probing for HIM-5::3xHA
167 by Western blotting (Figure 2B).
168
169 To begin to address the functional relevance of the interactions between DSB-1 and HIM-5,
170 we asked whether ectopic expression of HIM-5 could suppress the defects in bivalent
171 formation due to the loss of *dsb-1* or *dsb-2* functions. As shown in Figure 2C, ectopic HIM-5
172 very slightly reduced the number of univalents in either *dsb-1* or *dsb-2*. In *dsb-1* mutants. The

173 increase in *dsb-1* is seen by the shift from 12 to 11 DAPI staining bodies (corresponding to 12
174 univalents and 1 bivalent and 10 univalents, respectively) in ~20% of diakinesis nuclei. A
175 similar shift is seen in *dsb-2*, suggesting that HIM-5 provided one additional DSB/CO in these
176 mutant backgrounds. Consistent with little to no suppression, *pie-1::him-5* did not suppress the
177 hatching defects or male production in *dsb-2*. However, a slight suppression of the embryonic
178 lethality is seen with the *him-5p::him-5* transgene which is more highly expressed (Figure 2D).
179 The ability to suppress hatching but not the male production further supports the role of HIM-
180 5 in regulating total DSB numbers.
181
182 The inability of ectopic HIM-5 to strongly suppress *dsb-1* suggests that, unlike XND-1 and HIM-
183 17, DSB-1 does not regulate the expression of the *him-5* locus. However, using both live
184 imaging of HIM-5::GFP transgenes or anti-HA staining for endogenously-tagged HIM-5::3xHA,
185 we observed mislocalization of HIM-5 proteins in the *dsb-1* mutant background (Figure 2E).
186 Interestingly, the initial localization of HIM-5 is normal with nuclear localization in the transition
187 zone (leptotene/zygotene stage) nuclei. However, whereas in the wild type, HIM-5 protein
188 remains nuclear throughout early-mid pachytene; in *dsb-1* mutants, HIM-5 localizes to
189 cytoplasmic puncta at mid-pachytene. suggesting that DSB-1 (and/or its DSB-promoting
190 function) is required to retain HIM-5 in meiotic nuclei.
191
192 **Genetic interactions define four epistasis groups that contribute to DSB/CO formation.**
193 Having established interactions between subsets of the SPO-11 accessory factors in *C.*
194 *elegans*, we next wanted to perform more extensive genetic analyses between the known DSB
195 factors. To this end, we created double mutant combinations of alleles with partial DSB defects.
196 These included either weak loss-of-function alleles of essential DSB genes (*him-17, mre-11*)
197 or null alleles that reduce DSBs (*cep-1*, *dsb-2*, *rec-1*, *him-5*, and *parg-1*). Diakinesis oocytes
198 were analyzed in the single and double mutants by whole-mount fixation and DAPI staining

199 followed by confocal microscopy and 3D visualization. The chromosomes are highly
200 condensed at diakinesis, and six bivalents can be detected in wild-type worms. Univalents,
201 fusions, and DNA fragments can be seen in mutants with defects in DSB formation or their
202 repair into a CO, respectively (Chin & Villeneuve, 2001; Guo et al., 2022; Rosu et al., 2013).
203 We hypothesized that double mutant strains carrying mutations in genes that function in
204 different aspects of DSB induction would show more severe defects and have an increase in
205 univalent formation compared to single mutants. On the other hand, genes that function
206 together or at the same step of break induction should exhibit no or only mild enhancement of
207 the DSB defects.
208
209 Genetic epistasis was precluded in *dsb-1* and *dsb-3* since the single mutants already show a
210 complete absence of breaks (Hinman et al., 2021; Stamper et al., 2013). By contrast, *dsb-2*
211 mutant nuclei manifest an age-dependent loss in DSB capacity (Rosu et al., 2013; Stamper et
212 al., 2013) allowing us to analyze interactions between *dsb-2* and *cep-1, parg-1, him-17,* and
213 *rec-1* (Figure 3A and Figure S3A-D). As 1-day-old adults, *dsb-2* single mutants had ~50% of
214 diakinesis nuclei that contained 6 bivalents, ~30% with 7 DAPI-stained bodies (5 bivalents and
215 2 univalents), and ~20% with 8 or more DAPI-stained bodies. Single mutants of *cep-1*, *parg-*
216 *1,* and *rec-1* each had >90% of diakinesis nuclei with 6 bivalents, consistent with prior studies
217 (Chung et al., 2015; Janisiw et al., 2020; Mateo et al., 2016). In animals carrying *him-17(e2806)*
218 mutation, a weak allele of the otherwise essential locus for DSB formation, only ~50% of
219 mutant nuclei had 6 bivalents; the other 50% had 7 DAPI-stained bodies, reflecting the
220 requirement for this gene in CO formation on the X chromosome (Reddy & Villeneuve, 2004).
221 When *dsb-2* was combined with each of these mutations, an increased number of DAPI-
222 stained bodies and a concomitant decrease in the number of chiasmata were observed. These
223 results strongly suggest that *dsb-2* functions cooperatively with all four loci for the regulation
224 of meiotic CO formation.

225

226 Given that *rec-1, parg-1,* and *cep-1* fall in a separate epistasis group from *dsb-2*, we next
227 addressed whether these three genes function together or independently. All double mutant
228 permutations of *rec-1, parg-1,* and *cep-1* were analyzed, and in each case, the single and
229 double mutants were nearly indistinguishable from the single mutants, i.e., 6 bivalents (Figure
230 S3L-M). Therefore, we infer that these genes fall into the same epistasis group and therefore
231 likely function to control the same step in DSB/CO induction. Consistent with this interpretation,
232 when *rec-1, parg-1,* or *cep-1* were combined with other DSB gene mutations, including *him-*
233 *17*, they had similar effects, and the numbers of univalents were increased (Figures S3A, C,
234 D for Group 1; Figure S3E-G for Group 3; and Figure S3J, K for Group 4). Similar results have
235 previously been reported from our laboratories for double mutants with *him-5* (Chung et al.,
236 2015; Janisiw et al., 2020; Mateo et al., 2016).

237

238 *mre-11* functions in both DSB formation and subsequent DNA end resection (Chin &
239 Villeneuve, 2001), the latter as part of the MRE11-RAD50-NBS1/Xrs2 (MRN/X) resection
240 complex, the other proteins of which are encoded by the worm *rad-50* and *nbs-1* genes (Girard
241 et al., 2018; Hayashi et al., 2007). Null mutations in *mre-11* and *rad-50* completely abrogate
242 DSB induction. However, we were able to take advantage of a separation-of-function allele,
243 *mre-11(iow1),* that cannot perform its end-resection functions but can induce DSBs (Yin &
244 Smolikove, 2013). The *iow1* mutation causes chromosome fusions to appear in diakinesis
245 oocytes resulting from the aggregation of unprocessed DNA ends. While this allele makes
246 enough DSBs to cause aggregation of all chromosomes, we hypothesized that it might have a
247 minor impairment in DSB induction that would be revealed when combined with other DSB
248 mutations. If this were the case, the double mutants would make fewer breaks, leading to fewer
249 chromosome fusions and an increase in the number of DAPI-stained bodies/univalents.
250 Consistent with this hypothesis, *mre-11(iow1)* double mutants with each of the other DSB

251 mutations led to fewer fusions and more DAPI-stained bodies (Figure S3H-K; Figure 3A). Thus,
252 we propose that *mre-11,* and by extension *rad-50*, function in their own branch of the DSB/CO
253 pathway.
254
255 Surprisingly, a unique phenotype was observed in a subset of the *cep-1; mre-11* double
256 mutants. Our prior studies showed that *cep-1* functions redundantly with *him-5* to both ensure
257 DSB formation and promote downstream homologous recombination (HR) repair by preventing
258 non-homologous end joining (NHEJ) (Mateo et al., 2016). In that study, we reported that *cep-*
259 *1(lg12501)* is a separation-of-function allele that is defective in DSB formation. In the *cep-*
260 *1(lg12501);mre-11(iow-1)* double mutants, we observed mixed phenotypes: some nuclei had
261 12 DAPI-stained bodies, while others exhibited an exacerbation of the fusion defect (Figure
262 S4). We infer that the univalents indicate a synergistic effect between *mre-11* and *cep-1* for
263 DSB formation; the increase in fusions, on the other hand, may suggest that *cep-1(lg12501)*
264 is not fully wild-type for the DNA repair functions of CEP-1.
265
266 While each of the genes that we analyzed has reported roles in DSB formation, we wanted to
267 confirm that the observed increases in univalents in the double mutants were in fact due to
268 impairment in DSB induction and not to deficits in later steps of CO formation. Therefore, we
269 relied on an established assay to distinguish between these possibilities: we asked whether
270 the addition of exogenous breaks from gamma irradiation (IR) could suppress the univalent
271 phenotype by serving as a surrogate for SPO-11-induced DSBs (Dernburg et al., 1998).
272 Recent work has shown that 10Gy IR is able to produce up to ~20 DSBs per meiotic nucleus
273 (Lascarez-Lagunas et al., 2023), which is sufficient to ensure a CO on each chromosome (Mets
274 & Meyer, 2009). We analyzed the number of DAPI bodies with and without IR in a subset of
275 the double mutants where we observed synergistic effects (*dsb-2;parg-1*, *dsb-2;rec-1*, and *rec-*
276 *1;him-17*). When each of these double mutant strains was exposed to IR, the wild-type

277 phenotype of 6 bivalents was largely restored (Figure S5), supporting the conclusion that the
278 CO deficiency observed is triggered by defects in DSB formation.
279
280 **Protein-protein interactions between the DSB regulatory factors**
281 The genetic analyses described above defined four epistasis groups (Figure 3B). Using Y2H,
282 we next set out to determine whether interactions between groups could explain how the
283 different complexes come together to regulate DSB induction (Figure 3C-D). CEP-1 showed
284 auto-activation in both vectors and therefore was removed from further analysis. DSB-1, HIM-
285 17, and REC-1 also showed self-activation in the binding domain vector, therefore, only the
286 activation domain fusions were analyzed. Pairwise interactions between all remaining
287 combinations were then analyzed. HIM-5 displayed the most promiscuous Y2H interactions,
288 with strong interactions seen with MRE-11 and weak interactions as already discussed with
289 HIM-17 and DSB-1. XND-1 apart from interacting with HIM-17, also showed strong Y2H
290 interactions with REC-1. A recent study provided Y2H evidence supporting the idea that SPO-
291 11 interacts with DSB-1 (Hinman et al., 2021). Critically, our work supports and extends this
292 observation to show that DSB-1 is the only known accessory factor that interacts with SPO-11
293 in Y2H assays, cementing its role as a key determinant for DSB induction and explaining its
294 role in feedback controls (Stamper et al., 2013; Hinman et al., 2021; Guo et al., 2022).
295
296 To analyze more in-depth the Y2H interactions between DSB-1 and DSB-2, DSB-3, and SPO-
297 11, we looked for protein domains in DSB-1 that could be involved in these interactions.
298 Interestingly, DSB-1 has 5 “sticky” helices (helices 2-6 in Figure S6) that have the potential to
299 be implicated in protein-protein interactions. We first deleted all of these helices together by
300 introducing a deletion after L114 (DSB-1(1-114) in Figures 3E, F). We found that this truncated
301 version of DSB-1 loses the ability to interact with DSB-2 and DSB-3 but is still able to associate
302 with SPO-11. Moreover, when we only deleted the helices 3-6 but kept the helix 2 (DSB-1(1-

303 145)), we obtained the same results, suggesting that the Y2H interactions between DSB-1 and
304 DSB-2/DSB-3 is mediated by the C-terminal helices 3-6 and not helix 2. To prove this, we
305 created a truncated DSB-1 protein that only contains amino acids from P145 to the stop codon
306 (DSB-1(145-Ct)). Consistent with the deletion analysis, we observed that the C-terminal
307 domain is sufficient to promote associations with DSB-2 and DSB-3. This domain was also not
308 sufficient to promote the DSB-1/SPO-11 interaction (Figure 3E). These experiments
309 complement the results published by Villeneuve lab where they observed that the DSB-1 N-
310 terminus is the domain necessary for the DSB-1/SPO-11 (but not for the DSB-1/2/3) interaction
311 (Hinman et al., 2021). Together, these studies support the idea that the DSB-1/SPO-11 and
312 the DSB-1/2/3 interactions are mediated by distinct domains of DSB-1.
313

314 **DISCUSSION**

315 Across species, accessory factors collaborate with SPO-11 to regulate various aspects of DSB
316 formation, including the timing, placement, number, and persistence of DSB induction, as well
317 as the chromatin architecture at and around the break site (Arora et al., 2004; Cole et al., 2010;
318 Hinman et al., 2021; Kumar & de Massy, 2010; Panizza et al., 2011; Sasanuma et al., 2007;
319 Sommermeyer et al., 2013; Vrielynck et al., 2021). Here were present genetic, biochemical,
320 and cytological studies to develop the first comprehensive model for DSB regulation in a
321 metazoan. The *C. elegans* DSB complex appears to be comprised of four sub-groups (Figure
322 3B and 4) interconnected by interactions with HIM-5. Our results suggest two important roles
323 for HIM-5: first as the linchpin between the whole DSB complex, thereby ensuring the
324 coordination of the timing, placement, and number of DSBs (described in more detail below);
325 and second, as the determinant in X chromosome COs.

326

327 DSB-1 and DSB-2 are distant paralogs, and they are both orthologs of the budding yeast
328 Rec114 protein (Rosu et al., 2013; Stamper et al., 2013). On the other hand, DSB-3 is an
329 ortholog of yeast Mei4 (Hinman et al., 2021). In yeast and *Arabidopsis,* accessory proteins are
330 associated indirectly with Spo11/SPO11 through interactions with the TopVI/MTOPVIB subunit
331 (Arora et al., 2004; Kee & Keeney, 2002; Maleki et al., 2007; Robert et al., 2016; Vrielynck et
332 al., 2021). These differences between species underscore how conserved DSB proteins have
333 been co-opted to regulate different aspects of break induction. The lack of direct association
334 between SPO-11 and the other worm accessory factors points to DSB-1 as a hub for the
335 integration of various signals regulating break induction. For example, DSB-1 and DSB-2
336 persist longer on chromatin in strains that are defective in DSB induction (e.g. *mre-11; him-*
337 *17*), DNA repair, and SC formation. Their persistence has been suggested to be required to
338 maintain SPO-11 in a DSB-permissive state (Rosu et al., 2013; Stamper et al., 2013). This
339 was supported by studies that both identified ATM/ATR binding sites on these proteins (W. Li
340 & Yanowitz, 2019) and showed that phosphorylation of DSB-1 retains break competency (Guo
341 et al., 2022). Together, these data suggest that DSB-1 is responsible for inducing a second
342 wave of DSBs mediated by activation of ATL-1/ATM-1.

343

344 While DSB-1/-2/-3 are critical for CO formation, they predominantly localize on DNA loops with
345 little to no overlap (Hinman et al., 2021). Instead, a small fraction of these three proteins appear
346 to associate with the DNA axis, a localization that is consistent with the “tethered loop model”
347 for break induction in yeast and plants (Kee et al., 2004; Maleki et al., 2007; Panizza et al.,
348 2011; Sommermeyer et al., 2013; Tsai et al., 2020). Two accessory factors, MRE-11 and
349 PARG-1 are known interactors of the axis protein HTP-3 (Janisiw et al., 2020). Both proteins
350 interact either directly or indirectly with HIM-5, which physically associates with DSB-1, thereby
351 providing a mechanism to bring the loop-associated proteins to the axis.

352

353 MRE-11 and PARG-1 also have roles in both break formation and DNA repair. For PARG-1,
354 we show here that it functions together with REC-1 and CEP-1 based on the following data:
355 synthetic CO defects were seen in *cep-1;him-5*, *rec-1;him-5*, and *parg-1;him-5* (Chung et al.,
356 2015; Mateo et al., 2016 and this paper), but not in *rec-1;cep-1, rec-1;parg-1*, and *cep-1;parg-*
357 *1* double mutants; *dsb-2* mutant phenotypes are exacerbated by the loss of *rec-1*, *cep-1*
358 (Figure S3), and *parg*-1 (Janisiw et al., 2020). Interestingly, both CEP-1 and PARG-1 have
359 additional roles in promoting homologous recombination-mediated repair and/or preventing
360 alternative repair pathways (Janisiw, et al., 2020; Mateo et al., 2016). Therefore, we envision
361 that CEP-1, REC-1, and PARG-1 function together to promote DSBs and their repair into COs
362 at the chromosome axis. Since we also showed that the DSB defects in *mre-11* mutant animals
363 were enhanced by loss of *parg-1* or *rec-1* (Figure S3), we favor a model in which MRE-11 and
364 PARG-1 independently interact with the chromosome axis to ensure robust DSB formation
365 and/or repair. It is possible that MRE-11, which is essential for COs, is the major pathway for
366 tethering the loops to the axis, but further structural studies of these complexes are required.

367

368 The defects observed in *cep-1;him-5* (Mateo et al., 2016), and *rec-1;him-5* (Chung et al., 2015)
369 are both exacerbated by maternal age, similar to *dsb-2*. We envision that inputs from both
370 HIM-5 and DSB-2 converge on DSB-1 to ensure robust DSB formation across the lifespan.
371 This would also explain the synthetic defects in DSB formation between *dsb-2* and each of the
372 components in the *him-5* branch.

373

374

375 **TIMING of BREAKS**

376 Studies from multiple systems have elucidated mechanisms to coordinate the timing of DSBs
377 with the completion of meiosis, e.g. by CDK and Ddf4 phosphorylation in yeast (Murakami &
378 Keeney, 2008). In worms, REC-1 was previously shown to be a target of CDK and therefore it
379 was hypothesized that such a phosphorylation event would be critical to ensure that break
380 induction occurs after the completion of S phase (Chung et al., 2015). REC-1 and HIM-5
381 evolved from a gene duplication event in the *C. elegans* lineage; whereas the ancestral gene
382 in related nematodes has features of both proteins- although it shares greater homology with
383 HIM-5 (Chung et al., 2015). Thus, we hypothesize that the single ancestral REC-1/HIM-5
384 protein would be subject to CDK phosphorylation, which would then promote the assembly of
385 the complexes at the chromosome axis to promote break formation.

386

387 Timing also appears to be critical for CO outcomes. Studies in yeast show different outcomes
388 for early and late breaks (Joshi et al., 2015) and recent studies in worms indicate that later
389 breaks are needed for CO formation (Hicks et al., 2022) . We previously showed that *xnd-1*
390 mutants have altered DSB kinetics, showing elevated levels of DSB formation in
391 leptotene/zygotene (McClendon et al., 2016; Wagner et al., 2010). This function of XND-1 is
392 mediated, at least in part, by its effect on chromatin architecture. One possibility is that the
393 physical interaction that we show here between XND-1 and REC-1 couples the completion of
394 S phase to the activation of breaks within the correct chromatin environment, thus ensuring
395 their timely formation. In the absence of XND-1, increases in global histone acetylation (Gao
396 et al., 2015; Wagner et al., 2010) might allow SPO-11 easier access to the DNA. Another
397 possibility is that upon phosphorylation of REC-1 by CDK-1, REC-1 through PARG-1 tethers
398 XND-1 (the timer) to the axis, an event that restrains DSB formation.

399

400 **Chromatin and Meiotic Gene Transcription**

401 We also provide evidence for physical interactions between XND-1 and HIM-17, both by Y2H
402 and co-IP. HIM-17 appears to have a role in transcriptional regulation of DSB factors. Here we
403 show that ectopic expression of HIM-5 from the *pie-1* promoter, but not overexpression from
404 the endogenous *him-5* promoter, suppressed *him-17* phenotypes. This is similar to the rescue
405 we saw of *xnd-1* (McClendon et al., 2016) and suggests that both proteins contribute to the
406 expression of *him-5*. In addition, a recent study found that *him-17* regulates the expression of
407 ~300 germline-enriched genes, including *him-5, rec-1*, and *dsb-2*, (Carelli et al., 2022) whose
408 concomitant loss would be expected to abrogate break induction (Chung et al., 2015 and
409 Figure 3A and Figure S3). While its only role may be in transcriptional regulation, HIM-17 also
410 showed a weak physical interaction with HIM-5 in our Y2H assays. Although these interactions
411 were not confirmed by IP, it remains possible that these proteins have transient associations
412 that are unstable during IP or are not abundant. Together with observed changes in chromatin
413 structure and both DSB and CO distribution in *him-17* mutants(Nadarajan et al., 2021; Reddy
414 & Villeneuve, 2004), it is tempting to speculate that together with XND-1, HIM-17 helps to
415 create an environment permissive for SPO-11 binding and/or break formation. XND-1 and
416 HIM-17 may function together in this role or redundantly, perhaps through XND-1 interacting
417 with REC-1 and HIM-17 interacting with HIM-5, or in related species through interactions with
418 the REC-1/HIM-5 paralog.

419

420 **X/Autosome differences in DSB formation**

421 One of the conundrums that our data presents is the function of the HIM-5 protein. Our Y2H
422 and genetic data place this protein as a key mediator between the SPO-11-DSB complex and

423 the other accessory factors. However, mutations in *him*-5 preferentially impact CO formation
424 on the X chromosome (Broverman & Meneely, 1994; Hodgkin et al., 1979). Furthermore, *rec-*
425 *1;him-5* double mutants give an age-dependent severe loss of DSBs (like *dsb-2* mutants)
426 suggesting that the ancestral function of the protein may have a more profound effect on break
427 formation. While the X-specific phenotypes conferred by *him-5* mutation could suggest that
428 this chromosome is simply more sensitive to a reduction in the number of active SPO-11
429 complexes, the fact that mutations in *dsb-2* also reduce DSBs but without an X chromosome
430 bias argues against this interpretation. HIM-5 must have additional roles beyond directly
431 regulating the activation of SPO-11. We hypothesize that HIM-5 is the critical factor to ensure
432 that breaks occur on the X chromosome. In support of this, we show here that ectopic
433 expression of *him-5* can substantially rescue both the autosomal and X chromosomal defects
434 of *him-17* null mutations despite expression levels lower than endogenous *him-5*(McClendon
435 et al., 2016). The X chromosome-specific defects of *him-5* mutations might arise due to defects
436 in recruitment of DSB-1-2-3/SPO-11 to specific sites (hotspots) on the X or to an impaired
437 ability to coordinate the assembly of the DSB machinery on the axis of the X chromosome,
438 although other models can be envisioned.

439

440 **Concluding Remarks**

441 Our Y2H and IPs results show very strong protein-protein interaction between the different
442 DSB factors, however, it is also a fact that their localization along the gonads does not always
443 follow the same patterns. This can suggest that even when the proteins can interact, this
444 interaction might be time-space regulated depending on the role that each of these proteins
445 has during meiosis. Further studies are necessary to elucidate how these interactions arise
446 and change *in vivo.*

447 **METHODS**

448 **Culture and strains**

449 Worms were cultured on MyoB plates (Burns et al., 2006)) seeded with OP50 at 20°C, unless
450 otherwise noted (Brenner 1974). Mutant strains used in this study are listed in Supplemental
451 Material, Table S1. All strains were derived from the wild-type Bristol strain N2.

452

453 **Chromosome morphology analysis of diakinesis oocytes**

454 The numbers of DAPI-stained bodies present in diakinesis oocytes were assessed in intact
455 adult hermaphrodites at day 1 of adulthood (24 hours post-L4, unless otherwise specified).
456 Adults were fixed in Carnoy's fixative solution (60% ethanol, 30% chloroform, and 10%
457 glacial acetic acid) and stained with 4′,6-diamidino-2-phenylindole (DAPI) (10 mg/ml stock
458 diluted 1:50,000 in 1X Phosphate-buffered saline; PBS) for 15 minutes in a humid chamber.
459 Worms were mounted in Prolong Gold with DAPI, cured overnight at room temperature, and
460 stored at 4 °C prior to imaging either on a Nikon A1r confocal microscope or Leica Stellaris 5
461 confocal with an integrated White Light Laser (WLL). Diakinesis images were procured as
462 0.2μm per plain Z-stacks and visualized using Volocity 3-D Imaging Software for Nikon images
463 and LAS X for Leica images.

464

465 **γ-irradiation**

466 Worms of specified genotypes were exposed to 10Gy of γ-irradiation using a ^{137}Cs source
467 (Gammacell1000 Elite; Nordion International). Analysis of diakinesis oocytes by DAPI staining
468 was performed as described above at 28 h post-irradiation.

469

470 **Live imaging of *him-5* transgene**

471 Day 1 adults of *dsb-1; eaIs15* and day-2 adults of, *dsb-2; eaIs15* were placed on glass slides
472 and washed with M9 buffer (22 mM KH_2PO_4, 42 mM Na_2HPO_4, 85.5 mM NaCl, 1 mM $MgSO_4$)
473 to remove residual bacteria. Then the worms were incubated for 20 min with a solution of
474 DRAQ5 (1:2000 in M9), washed for 1 minute with M9, and the gonads dissected in M9 with
475 0.1 µl of 1mM levamisole. Images were taken with a Leica Stellaris 5 confocal with a WLL.

476

477 **Yeast two-hybrid assay**

478 *GAL4* activating domain– (pGAD-C1) and binding domain (pGBD-C1)–expressing vectors
479 were co-transformed into the PJ69-4a yeast strain and selected by growth on SC-LEU-TRP
480 medium. Three to five transformants were grown to early log phase to 0.2 OD_{600}, and 5 µl were
481 spotted onto medium to select for the plasmids (SC-LEU-TRP; loading control) or onto medium
482 to select for expression of the reporter *HIS3* gene (SC-LEU-TRP-HIS; which is indicative of a
483 yeast-two-hybrid interaction). Plates were incubated for 72 hours at 30°C and imaged. The
484 experiments were done in triplicate and empty vectors in the activating and binding domains
485 were used as negative controls.

486

487 **Co-Immunoprecipitation and Western Blot**

488 In order to perform co-immunoprecipitation experiments, synchronized *GFP::dsb-1; him-*
489 *5::3xHA* and *him-5::3xHA* or *him-17::3xHA; him-5::GFP::3xFLAG* and *him-5::GFP::3xFLAG*
490 strains were grown until young adult stage (24h post-L4) and nuclear protein fractionation was

491 executed as previously shown (Silva et al.; 2014). The chromatin-bound fraction was
492 generated upon Benzonase digestion (25U/100 ml of extract for 1h at 4°C). 2 mg of nuclear
493 extract (nuclear-soluble and chromatin-bound fractions were pooled together) was incubated
494 with Agarose GFP traps (Chromotek) or anti-HA Affinity Matrix (Roche) in Buffer D (20mM
495 HEPES pH 7.9, 150mM KCl, 20% glycerol, 0.2mM EDTA, 0.2% Triton X-100 and 1x complete
496 Roche inhibitor) overnight at 4°C. The following day, the agarose beads were recovered by
497 centrifugation at 7500 rpm for 2´at 4°C and extensively washed with Buffer D at room
498 temperature. After the final wash, the beads were resuspended in 40 ml of 2x Laemmli Buffer
499 and boiled for 10´, after which they were spun at maximum speed for 1´ and the whole eluate
500 was loaded on a precast 4-20% gradient acrylamide gel. Proteins were transferred on a
501 nitrocellulose membrane for 90 minutes at 4°C at 100V and blocked for 1h at room temperature
502 in 1x TBST containing 5% BSA. Mouse monoclonal anti-HA (Cell Signaling), chicken
503 polyclonal anti-GFP (AbCam), mouse monoclonal anti-FLAG HRP-conjugated (Sigma), and
504 polyclonal anti-XND-1 (Wagner et al., 2010) antibodies were diluted in blocking solution at
505 1:1000, 1:5000, 1:2000 and 1:2500 respectively and left to incubate overnight at 4°C. Washes
506 were performed in 1x TBST and anti-mouse, anti-chicken, and anti-guinea pig HRP-conjugated
507 secondary antibodies (ThermoFisher) were diluted 1:10,000 in 1x TBST containing 5% milk
508 for 1h at room temperature. After several washes in 1xTBST, the membrane was incubated
509 with Clarity Max ECL (BioRad) and imaged with a G-Box (Syngene).

510

511 **Immunofluorescence and STED imaging**

512 Gonads were dissected from 1-day adults of *him-17::3xHA* worms in 1X sperm salts (50 mM
513 PIPES pH 7.0, 25 mM KCl, 1 mM MgSO4, 45 mM NaCl, and 2 mM CaCl2) with 1 mM
514 levamisole and fixed in 1% paraformaldehyde diluted in 1X sperm salts for 5 min in a humid

515 chamber. Slides were then frozen on a metal block on dry ice for at least 10 min prior to
516 flicking off the coverslip and immersing in 100% ethanol at −20° C for 2 min. Slides were then
517 washed in PBSTB [1XPBS with 0.1% Tween and 0.1% bovine serum albumin (BSA)], and
518 incubated overnight at 4°C with primary antibody: mouse anti-HA (Cell Signaling), guinea pig
519 anti-XND-1(Wagner et al., 2010), and rabbit anti-HTP-3 (Das et al., 2022) (all diluted 1:2000
520 in PBST). The next day, slides were washed 3X in PBSTB for 10 min and incubated with
521 secondary antibodies: anti-mouse Alexa 488 (Molecular Probes), anti-guinea pig 633, and
522 goat anti-rabbit Alexa 568 (Invitrogen, all diluted 1:2000 in PBSTB) for 2 h at room
523 temperature in the dark. Slides were then washed 2 X 10 min in PBSTB, mounted in Prolong
524 Gold without DAPI (Invitrogen) and put in the dark to cure overnight before imaging. The
525 images were taken using a Stellaris8 TauSTED equipped with three depletion lines.

526

527 **HIM-17 and mass spectrometry analysis**

528 Preparation and freezing of synchronized worms were carried out as in Cheeseman et al.,
529 (2004) except that worms were grown on 8P plates seeded with the *E. coli* strain NA22 at room
530 temperature. Worm lysis was carried out by grinding worm pellets in liquid nitrogen and
531 subsequent sonication (Diagenode) was performed with the following settings: 3x 5 cycles on
532 high with 30 seconds on and 30 seconds off. Lysate was centrifuged for 45 minutes at 15000
533 rpm at 4°C. To avoid unspecific protein binding the worm lysate was pre-cleared by incubation
534 to uncoupled agarose beads (Chromotek, bab-20) for 1 hour at 4°C. Pre-cleared worm lysate
535 was incubated with GFP-trap (Chromotek, gta-20) for 3 hours at 4°C. Beads were washed 3
536 times with lysis buffer containing proteinase inhibitors (Roche) and 7 times with lysis buffer
537 without proteinase inhibitors. Proteins were eluted by adding 40 µl 2xLSB and boiling for 5 min
538 at 95°C. Protein precipitation was carried out using ProteoExtract Protein Precipitation Kit

539 (EMD Millipore, 539180-1KIT) according to the manufacturer's protocol and submitted for MS
540 analysis to the Taplin Biological Mass Spectrometry Facility.

541

542 **Acknowledgments**

543 We are grateful to P. Carlton for the *GFP::dsb-1* strain. This work was funded by
544 R01GM104007 and S10 grant # 1S10OD030404 to JLY; the Czech Science Foundation (23-
545 04918S) to NS; NIH grant R01GM072551 to M.P.C.; R01ES030335 and Penn Center for
546 Genome Integrity to KAB.

547

548

549 **Bibliography**

550 Arora, C., Kee, K., Maleki, S., & Keeney, S. (2004). Antiviral protein Ski8 is a direct partner of
551 Spo11 in meiotic DNA break formation, independent of its cytoplasmic role in RNA
552 metabolism. *Molecular Cell*, *13*(4), 549–559. https://doi.org/10.1016/S1097-
553 2765(04)00063-2
554 Bergerat, A., De Massy, B., Gadelle, D., Varoutas, P.-C., Nicolas, A., & Forterre, P. (1997).
555 An atypical topoisomerase II from Archaea with implications for meiotic recombination.
556 *Nature*, *386*(6623), 414–417.
557 Bouuaert, C. C., Tischfield, S. E., Pu, S., Mimitou, E. P., Arias-palomo, E., Berger, J. M., &
558 Keeney, S. (2021). *Structural and functional characterization of the Spo11 core complex*.
559 *28*(January).
560 Broverman, S. A., & Meneely, P. M. (1994). Meiotic mutants that cause a polar decrease in
561 recombination on the X chromosome in Caenorhabditis elegans. *Genetics*, *136*(1), 119–
562 127.
563 Burns, A. R., Kwok, T. C. Y., Howard, A., Houston, E., Johanson, K., Chan, A., Cutler, S. R.,
564 McCourt, P., & Roy, P. J. (2006). High-throughput screening of small molecules for
565 bioactivity and target identification in Caenorhabditis elegans. *Nature Protocols*, *1*(4),
566 1906–1914. https://doi.org/10.1038/nprot.2006.283
567 Cheeseman, I. M., Niessen, S., Anderson, S., Hyndman, F., Yates, J. R., Oegema, K., &
568 Desai, A. (2004). A conserved protein network controls assembly of the outer
569 kinetochore and its ability to sustain tension. *Genes and Development*, *18*(18), 2255–
570 2268. https://doi.org/10.1101/gad.1234104
571 Chin, G. M., & Villeneuve, A. M. (2001). C. elegans mre-11 is required for meiotic
572 recombination and DNA repair but is dispensable for the meiotic G2 DNA damage
573 checkpoint. *Genes and Development*, *15*(5), 522–534.
574 https://doi.org/10.1101/gad.864101
575 Chung, G., Rose, A. M., Petalcorin, M. I. R., Martin, J. S., Kessler, Z., Sanchez-Pulido, L.,
576 Ponting, C. P., Yanowitz, J. L., & Boulton, S. J. (2015). REC-1 and HIM-5 distribute
577 meiotic crossovers and function redundantly in meiotic double-strand break formation in
578 Caenorhabditis elegans. *Genes and Development*, *29*(18), 1969–1979.
579 https://doi.org/10.1101/gad.266056.115
580 Cole, F., Keeney, S., & Jasin, M. (2010). Evolutionary conservation of meiotic DSB proteins:
581 More than just Spo11. *Genes and Development*, *24*(12), 1201–1207.
582 https://doi.org/10.1101/gad.1944710
583 Das, D., Trivedi, S., Blazícková, J., Arur, S., & Silva, N. (2022). Phosphorylation of HORMA-
584 domain protein HTP-3 at Serine 285 is dispensable for crossover formation. *G3*, *12*(5),
585 jkac079.
586 Dernburg, A. F., McDonald, K., Moulder, G., Barstead, R., Dresser, M., & Villeneuve, A. M.
587 (1998). Meiotic recombination in C. elegans initiates by a conserved mechanism and is
588 dispensable for homologous chromosome synapsis. *Cell*, *94*(3), 387–398.
589 https://doi.org/10.1016/S0092-8674(00)81481-6
590 Dungan, J. (2002). Genetics in medicine. *Fertility and Sterility*, *77*(5), 1091.
591 Gao, J., Kim, H. M., Elia, A. E., Elledge, S. J., & Colaiácovo, M. P. (2015). NatB Domain-
592 Containing CRA-1 Antagonizes Hydrolase ACER-1 Linking Acetyl-CoA Metabolism to
593 the Initiation of Recombination during C. elegans Meiosis. *PLoS Genetics*, *11*(3), 1–28.
594 https://doi.org/10.1371/journal.pgen.1005029
595 Girard, C., Roelens, B., Zawadzki, K. A., & Villeneuve, A. M. (2018). Interdependent and
596 separable functions of Caenorhabditis elegans MRN-C complex members couple
597 formation and repair of meiotic DSBs. *Proceedings of the National Academy of Sciences*

598 *of the United States of America*, *115*(19), E4443–E4452.
599 https://doi.org/10.1073/pnas.1719029115
600 Guo, H., Stamper, E. L., Sato-Carlton, A., Shimazoe, M. A., Li, X., Zhang, L., Stevens, L.,
601 Tam, J., Dernburg, A. F., & Carlton, P. M. (2022). Phosphoregulation of DSB-1 mediates
602 control of meiotic double-strand break activity. *BioRxiv*, 1–30.
603 https://doi.org/10.1101/2022.02.16.480793
604 Hassold, T., Hall, H., & Hunt, P. (2007). The origin of human aneuploidy: where we have
605 been, where we are going. *Human Molecular Genetics*, *16*(R2), R203--R208.
606 Hayashi, M., Chin, G. M., & Villeneuve, A. M. (2007). C. elegans germ cells switch between
607 distinct modes of double-strand break repair during meiotic prophase progression. *PLoS*
608 *Genetics*, *3*(11), 2068–2084. https://doi.org/10.1371/journal.pgen.0030191
609 Henderson, K. A., Kee, K., Maleki, S., Santini, P. A., & Keeney, S. (2006). Cyclin-dependent
610 kinase directly regulates initiation of meiotic recombination. *Cell*, *125*(7), 1321–1332.
611 Hinman, A. W., Yeh, H. Y., Roelens, B., Yamaya, K., Woglar, A., Bourbon, H. M. G., Chi, P.,
612 & Villeneuve, A. M. (2021). Caenorhabditis elegans DSB-3 reveals conservation and
613 divergence among protein complexes promoting meiotic double-strand breaks.
614 *Proceedings of the National Academy of Sciences of the United States of America*,
615 *118*(33), 1–12. https://doi.org/10.1073/pnas.2109306118
616 Hodgkin, J., Horvitz, H. R., & Brenner, S. (1979). Nondisjunction Mutants of the Nematode
617 CAENORHABDITIS ELEGANS. *Genetics*, *91*(1), 67–94.
618 http://www.pubmedcentral.nih.gov/articlerender.fcgi?artid=1213932&tool=pmcentrez&re
619 ndertype=abstract
620 Janisiw, E., Raices, M., Balmir, F., Paulin, L. F., Baudrimont, A., von Haeseler, A., Yanowitz,
621 J. L., Jantsch, V., & Silva, N. (2020). Poly(ADP-ribose) glycohydrolase coordinates
622 meiotic DNA double-strand break induction and repair independent of its catalytic
623 activity. *Nature Communications*, *11*(1), 1–15. https://doi.org/10.1038/s41467-020-
624 18693-1
625 Joshi, N., Brown, M. S., Bishop, D. K., & Börner, G. V. (2015). Gradual implementation of the
626 meiotic recombination program via checkpoint pathways controlled by global DSB levels.
627 *Molecular Cell*, *57*(5), 797–811. https://doi.org/10.1177/0022146515594631.Marriage
628 Kee, K., & Keeney, S. (2002). *Meiotic Recombination in Saccharomyces cerevisiae*.
629 *122*(January), 111–122.
630 Kee, K., Protacio, R. U., Arora, C., & Keeney, S. (2004). Spatial organization and dynamics
631 of the association of Rec102 and Rec104 with meiotic chromosomes. *EMBO Journal*,
632 *23*(8), 1815–1824. https://doi.org/10.1038/sj.emboj.7600184
633 Keeney, S. (2008). Spo11 and the formation of DNA double-strand breaks in meiosis.
634 *Genome Dynamics and Stability*, *2*, 81–123. https://doi.org/10.1007/7050_2007_026
635 Keeney, S., Giroux, C. N., & Kleckner, N. (1997). Meiosis-specific DNA double-strand breaks
636 are catalyzed by Spo11, a member of a widely conserved protein family. *Cell*, *88*(3),
637 375–384. https://doi.org/10.1016/S0092-8674(00)81876-0
638 Kumar, R., Bourbon, H. M., & de Massy, B. (2010). Functional conservation of Mei4 for
639 meiotic DNA double-strand break formation from yeasts to mice. *Genes and*
640 *Development*, *24*(12), 1266–1280. https://doi.org/10.1101/gad.571710
641 Kumar, R., & de Massy, B. (2010). Initiation of meiotic recombination in mammals. *Genes*,
642 *1*(3), 521–549. https://doi.org/10.3390/genes1030521
643 Lam, I., & Keeney, S. (2015). Mechanism and regulation of meiotic recombination initiation.
644 *Cold Spring Harbor Perspectives in Biology*, *7*(1).
645 https://doi.org/10.1101/cshperspect.a016634
646 Lascarez-Lagunas, L. I., Martinez-Garcia, M., Nadarajan, S., Diaz-Pacheco, B. N., Berson,
647 E., & Colaiácovo, M. P. (2023). Chromatin landscape, DSB levels, and cKU-70/ 80

contribute to patterning of meiotic DSB processing along chromosomes in C. elegans. *PLoS Genetics*, *19*(1), 1–27. https://doi.org/10.1371/journal.pgen.1010627

Li, J., Hooker, G. W., & Roeder, G. S. (2006). Saccharomyces cerevisiae Mer2, Mei4 and Rec114 form a complex required for meiotic double-strand break formation. *Genetics*, *173*(4), 1969–1981. https://doi.org/10.1534/genetics.106.058768

Li, W., & Yanowitz, J. L. (2019). ATM and ATR influence meiotic crossover formation through antagonistic and overlapping functions in caenorhabditis elegans. *Genetics*, *212*(2), 431–443. https://doi.org/10.1534/genetics.119.302193

Maleki, S., Neale, M. J., Arora, C., Henderson, K. A., & Keeney, S. (2007). Interactions between Mei4, Rec114, and other proteins required for meiotic DNA double-strand break formation in Saccharomyces cerevisiae. *Chromosoma*, *116*(5), 471–486. https://doi.org/10.1007/s00412-007-0111-y

Martini, E., Diaz, R. L., Hunter, N., & Keeney, S. (2006). Crossover homeostasis in yeast meiosis. *Cell*, *126*(2), 285–295.

Mateo, A. R. F., Kessler, Z., Jolliffe, A. K., McGovern, O., Yu, B., Nicolucci, A., Yanowitz, J. L., & Derry, W. B. (2016). The p53-like Protein CEP-1 Is Required for Meiotic Fidelity in C. Elegans. *Current Biology*, *26*(9), 1148–1158. https://doi.org/10.1016/j.cub.2016.03.036

McClendon, T. B., Mainpal, R., Gandhi Amrit, F. R., Krause, M. W., Ghazi, A., & Yanowitz, J. L. (2016). X Chromosome Crossover Formation and Genome Stability in Caenorhabditis elegans Are Independently Regulated by xnd-1. *G3: Genes|Genomes|Genetics*, *6*(December), 3913–3925. https://doi.org/10.1534/g3.116.035725

Meneely, P. M., McGovern, O. L., Heinis, F. I., & Yanowitz, J. L. (2012). Crossover distribution and frequency are regulated by him-5 in caenorhabditis elegans. *Genetics*, *190*(4), 1251–1266. https://doi.org/10.1534/genetics.111.137463

Mets, D. G., & Meyer, B. J. (2009). Condensins Regulate Meiotic DNA Break Distribution, thus Crossover Frequency, by Controlling Chromosome Structure. *Cell*, *139*(1), 73–86. https://doi.org/10.1016/j.cell.2009.07.035

Murakami, H., & Keeney, S. (2008). Regulating the formation of DNA double-strand breaks in meiosis. *Genes and Development*, *22*(3), 286–292. https://doi.org/10.1101/gad.1642308

Nadarajan, S., Altendorfer, E., Saito, T. T., Martinez-Garcia, M., & Colaiácovo, M. P. (2021). HIM-17 regulates the position of recombination events and GSP-1/2 localization to establish short arm identity on bivalents in meiosis. *Proceedings of the National Academy of Sciences of the United States of America*, *118*(17), 1–10. https://doi.org/10.1073/pnas.2016363118

Panizza, S., Mendoza, M. A., Berlinger, M., Huang, L., Nicolas, A., Shirahige, K., & Klein, F. (2011). Spo11-accessory proteins link double-strand break sites to the chromosome axis in early meiotic recombination. *Cell*, *146*(3), 372–383. https://doi.org/10.1016/j.cell.2011.07.003

Prieler, S., Penkner, A., Borde, V., & Klein, F. (2005). The control of Spo11's interaction with meiotic recombination hotspots. *Genes and Development*, *19*(2), 255–269. https://doi.org/10.1101/gad.321105

Reddy, K. C., & Villeneuve, A. M. (2004). C. elegans HIM-17 links chromatin modification and competence for initiation of meiotic recombination. *Cell*, *118*(4), 439–452.

Robert, T., Nore, A., Brun, C., Maffre, C., Crimi, B., Bourbon, H.-M. H., Massy, B. De, Guichard, V., Bourbon, H.-M. H., & De Massy, B. (2016). The TopoVIB-Like protein family is required for meiotic DNA double-strand break formation. *Science*, *351*(6276), 943–949.

Rose, A. M., & Baillie, D. L. (1979). A mutation in Caenorhabditis elegans that increases recombination frequency more than threefold. *Nature*, *281*(5732), 599–600.

Rosu, S., Zawadzki, K. A., Stamper, E. L., Libuda, D. E., Reese, A. L., Dernburg, A. F., & Villeneuve, A. M. (2013). The C. elegans DSB-2 protein reveals a regulatory network that controls competence for meiotic DSB formation and promotes crossover assurance. *PLoS Genetics*, *9*(8), e1003674.

Sasanuma, H., Murakami, H., Fukuda, T., Shibata, T., Nicolas, A., & Ohta, K. (2007). Meiotic association between Spo11 regulated by Rec102, Rec104 and Rec114. *Nucleic Acids Research*, *35*(4), 1119–1133. https://doi.org/10.1093/nar/gkl1162

Sommermeyer, V., Béneut, C., Chaplais, E., Serrentino, M. E., & Borde, V. (2013). Spp1, a Member of the Set1 Complex, Promotes Meiotic DSB Formation in Promoters by Tethering Histone H3K4 Methylation Sites to Chromosome Axes. *Molecular Cell*, *49*(1), 43–54. https://doi.org/10.1016/j.molcel.2012.11.008

Stamper, E. L., Rodenbusch, S. E., Rosu, S., Ahringer, J., Villeneuve, A. M., & Dernburg, A. F. (2013). Identification of DSB-1, a Protein Required for Initiation of Meiotic Recombination in Caenorhabditis elegans, Illuminates a Crossover Assurance Checkpoint. *PLoS Genetics*, *9*(8), 1–18. https://doi.org/10.1371/journal.pgen.1003679

Tsai, B., Liu, W., Dong, D., Shi, K., Chen, L., & Gao, N. (2020). Phase separation of Mer2 organizes the meiotic loop-axis structure of chromatin during meiosis I. *BioRxiv*, 2020.12.15.422856. https://doi.org/10.1101/2020.12.15.422856

Vrielynck, N., Schneider, K., Rodriguez, M., Sims, J., Chambon, A., Hurel, A., De Muyt, A., Ronceret, A., Krsicka, O., Mézard, C., Schlögelhofer, P., & Grelon, M. (2021). Conservation and divergence of meiotic DNA double strand break forming mechanisms in Arabidopsis thaliana. *Nucleic Acids Research*, *49*(17), 9821–9835. https://doi.org/10.1093/nar/gkab715

Wagner, C. R., Kuervers, L., Baillie, D., & Yanowitz, J. L. (2010). xnd-1 regulates the global recombination landscape in C. elegans. *Nature*, *467*(7317), 839–843. https://doi.org/doi:10.1038/nature09429

Yeh, H. Y., Lin, S. W., Wu, Y. C., Chan, N. L., & Chi, P. (2017). Functional characterization of the meiosis-specific DNA double-strand break inducing factor SPO-11 from C. elegans. *Scientific Reports*, *7*(1), 1–11. https://doi.org/10.1038/s41598-017-02641-z

Yin, Y., & Smolikove, S. (2013). Impaired Resection of Meiotic Double-Strand Breaks Channels Repair to Nonhomologous End Joining in Caenorhabditis elegans. *Molecular and Cellular Biology*, *33*(14), 2732–2747. https://doi.org/10.1128/mcb.00055-13

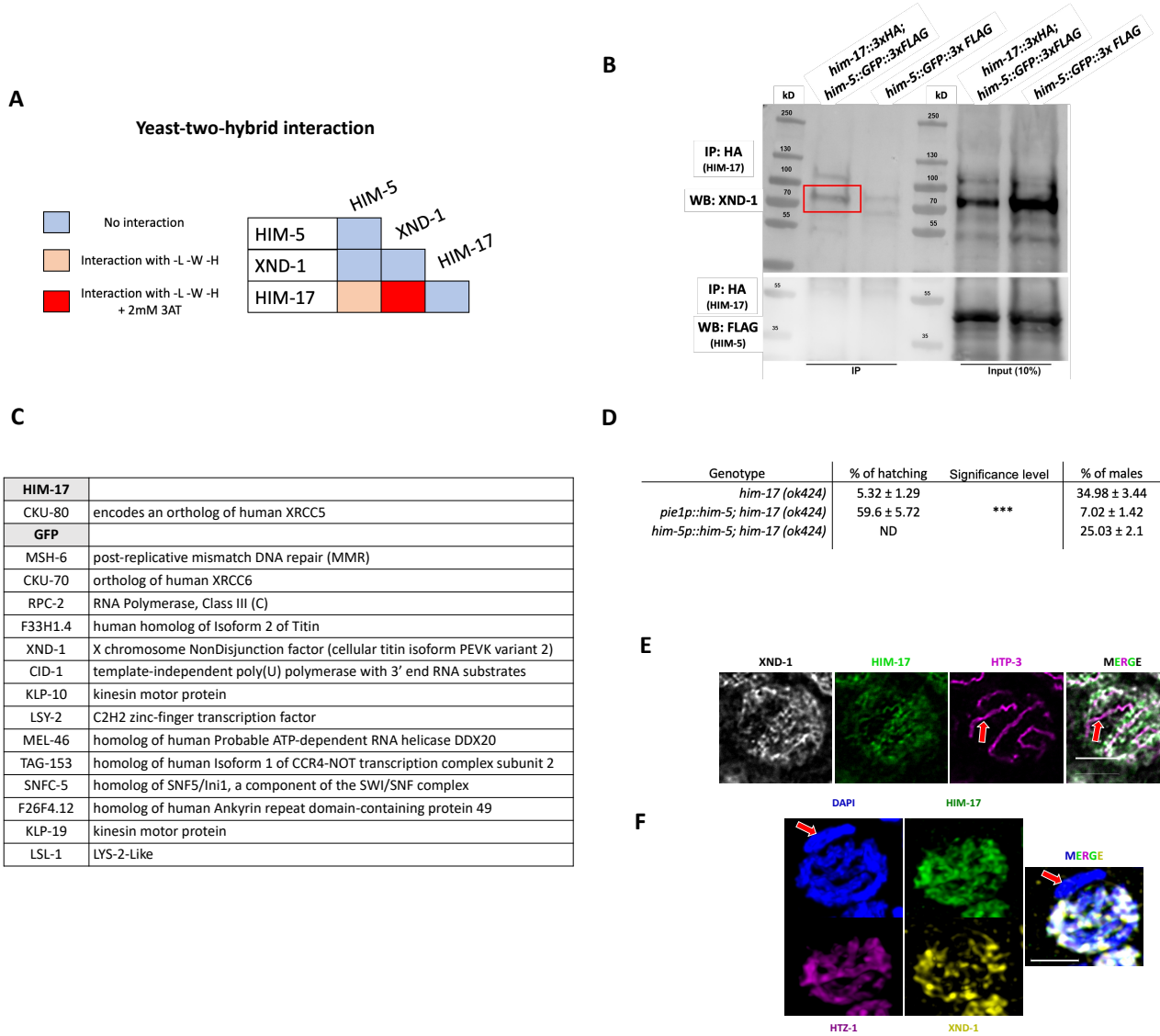

HIM-17	
CKU-80	encodes an ortholog of human XRCC5
GFP	
MSH-6	post-replicative mismatch DNA repair (MMR)
CKU-70	ortholog of human XRCC6
RPC-2	RNA Polymerase, Class III (C)
F33H1.4	human homolog of Isoform 2 of Titin
XND-1	X chromosome NonDisjunction factor (cellular titin isoform PEVK variant 2)
CID-1	template-independent poly(U) polymerase with 3' end RNA substrates
KLP-10	kinesin motor protein
LSY-2	C2H2 zinc-finger transcription factor
MEL-46	homolog of human Probable ATP-dependent RNA helicase DDX20
TAG-153	homolog of human Isoform 1 of CCR4-NOT transcription complex subunit 2
SNFC-5	homolog of SNF5/Ini1, a component of the SWI/SNF complex
F26F4.12	homolog of human Ankyrin repeat domain-containing protein 49
KLP-19	kinesin motor protein
LSL-1	LYS-2-Like

Genotype	% of hatching	Significance level	% of males	Significance level
him-17 (ok424)	5.32 ± 1.29		34.98 ± 3.44	
pie1p::him-5; him-17 (ok424)	59.6 ± 5.72	***	7.02 ± 1.42	***
him-5p::him-5; him-17 (ok424)	ND		25.03 ± 2.1	NS

Figure 1: XND-1 and HIM-17 interact and are predominantly localized away from the DNA axis. A) Summary of the yeast two-hybrid assay results. The complete set of results is given in Figure S1A. **B)** Western blot analysis of endogenous XND-1 (top) and HIM-5::GFP::FLAG (bottom) on HA pull-downs performed in *him-17::3xHA;him-5::GFP::3xFLAG* strain. Analysis was performed in biological duplicates. **C)** Mass spectrometry results of GFP pulldowns of HIM-17::GFP. IP/MS analysis was performed in duplicate and corrected for nonspecific binding of proteins bound to GFP trap beads. **D)** Quantification of embryonic viability (hatching rates) and frequencies of male offspring among the progeny of the indicated genotypes. Data are shown as mean +/- SD; NS stands for not significant; **** $p < 0.0001$, n= number of P_0 parents whose brood was examined. **E)** Representative STED images of mid-pachytene stage nuclei showing substantial overlap of XND-1 and HIM-17 on DNA not at the chromosome axis (stained with HTP-3). The X chromosome is not stained by either XND-1 and HIM-17 (red arrow). **F)** Representative confocal images showing co-localization of XND-1 and HIM-17 with an autosome-enriched variant histone, HTZ-1. Red arrow indicates the X chromosome. Scale bars = 2μm.

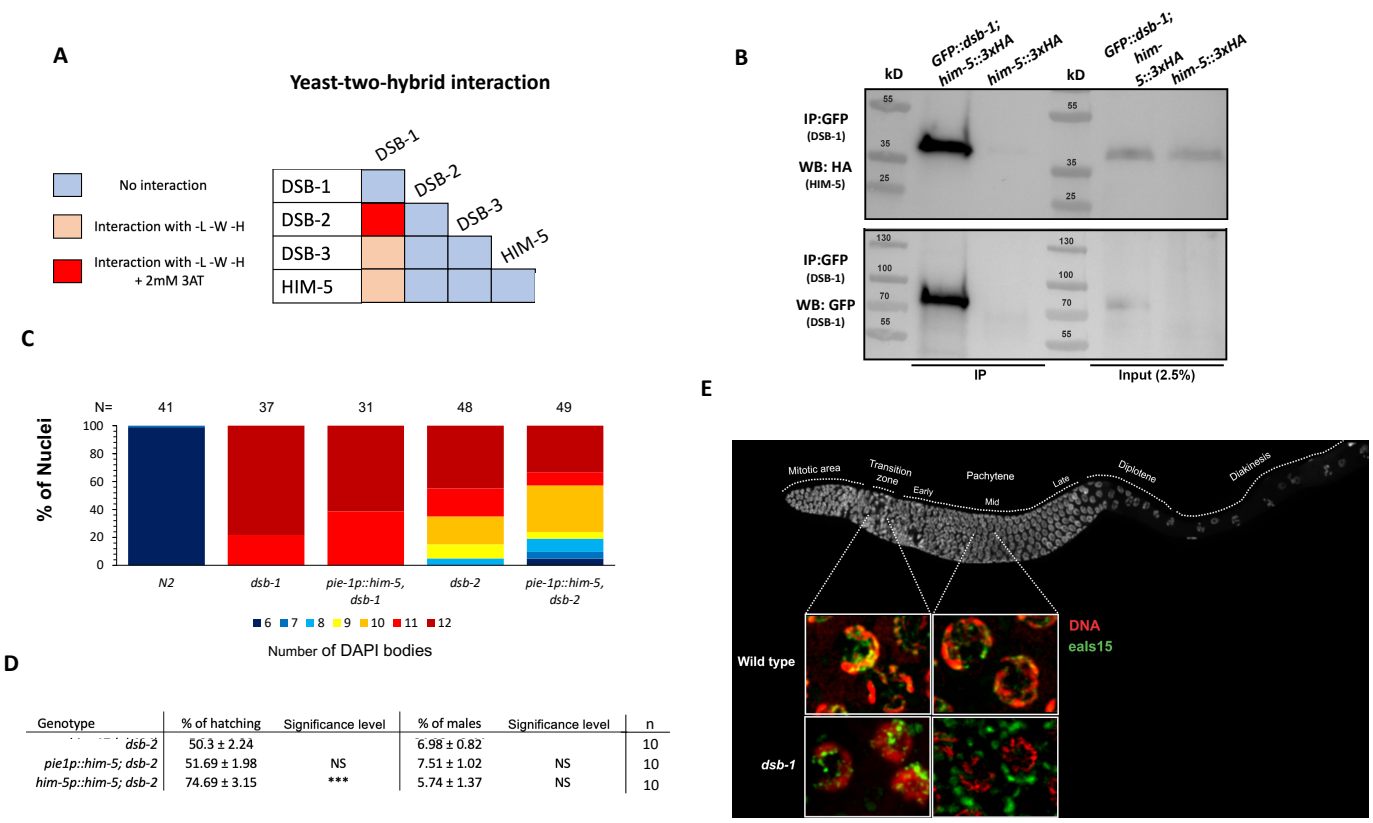

D

Genotype	% of hatching	Significance level	% of males	Significance level	n
dsb-2	50.3 ± 2.24		6.98 ± 0.82		10
pie1p::him-5; dsb-2	51.69 ± 1.98	NS	7.51 ± 1.02	NS	10
him-5p::him-5; dsb-2	74.69 ± 3.15	***	5.74 ± 1.37	NS	10

Figure 2: DSB-1 associates with HIM-5 and regulates its localization A) Summary of the yeast two-hybrid assay results. The complete set of results is given in Figure S1A. **B)** Western blot analysis of GFP pull-downs performed in *GFP::dsb-1;him-5::3XHA* strain showing co-IP of HA-tagged HIM-5 proteins. Analysis was performed in biological duplicates. **C)** Quantification of DAPI-stained bodies at diakinesis for the indicated genotypes. Colors correspond to the number of DAPI-stained bodies shown in the key below. **D)** Quantification of embryonic viability (hatching rates) and frequencies of male offspring among the progeny of the indicated genotypes. Data are shown as mean +/- SD; NS stands for not significant; **** $p < 0.0001$, n= number of P_0 parents whose brood was examined. **E) Top:** *C. elegans* gonad fixed and stained with DAPI to show the organization and distribution of the nuclei along the Prophase I. **Bottom:** live images of nuclei in the transition zone (leptotene-zygotene) and middle-pachytene. *eals15 (Ppie-1::him-5)* is visualized in freshly dissected gonads by GFP fluorescence (green), and DNA by DRAQ5 (red). In *dsb-1* mutants, HIM-5 is located is nuclear in the transition zone and becomes located in cytoplasmic puncta by middle pachytene.

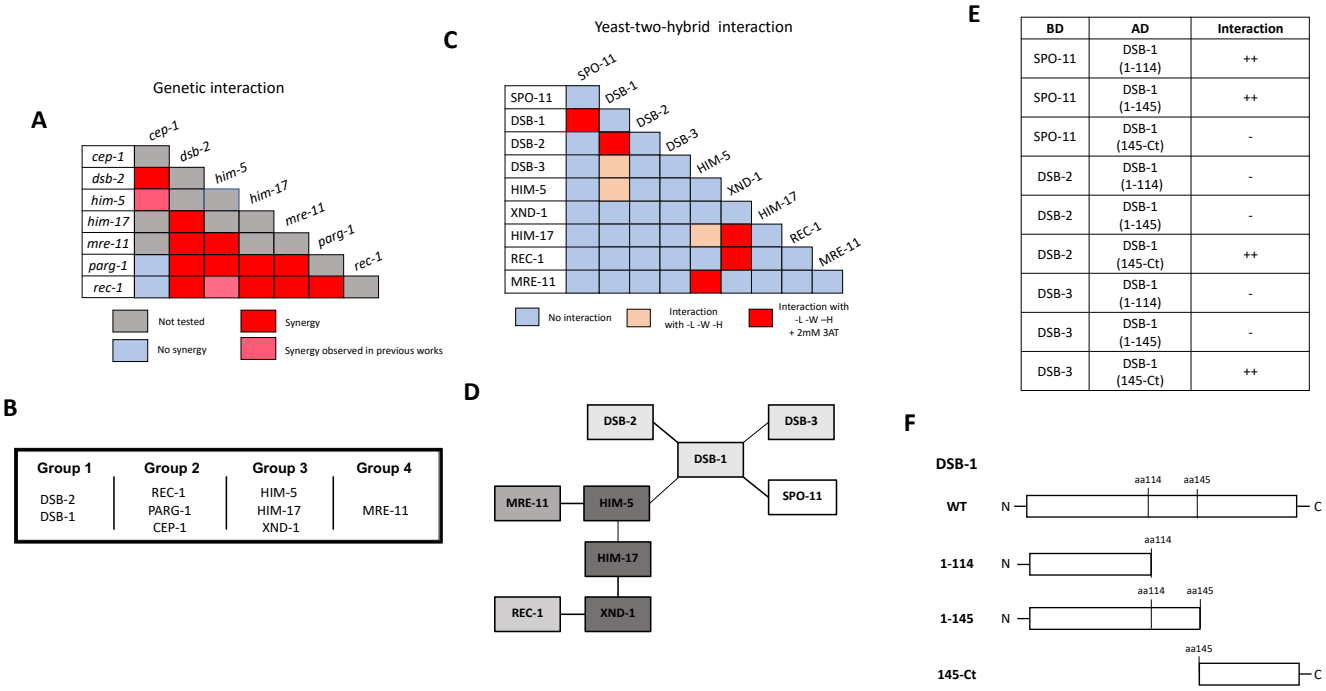

Figure 3: Genetic and protein-protein interaction studies show evidence of DSB protein sub-complexes in *C. elegans.* A) Summary of the genetic interaction results. The complete set of results is given in Figure S3. **B)** Genetic groups are based on data presented here and previously published (Chung et al., 2015; Mateo et al., 2016; McClendon et al., 2016; Janisiw et al., 2020). **C)** Summary of the yeast two-hybrid assay results. The complete set of results is given in Figure S1A. **D)** Schematic representation of the interaction network based on Y2H interactions. Thick line: Strong interaction between two proteins. Thin line: weak interaction between two proteins. **E)** Different DSB-1 constructs (detailed in F) were used to analyze yeast-two-hybrid interactions with SPO-11, DSB-2, and DSB-3. **F)** Scheme representation of the wild-type DSB-1 structure, and the different truncations used in **E)** For more details about the DSB-1 sequence, protein structure, and deletions used in these experiments, see **Figure S5.**

788

789

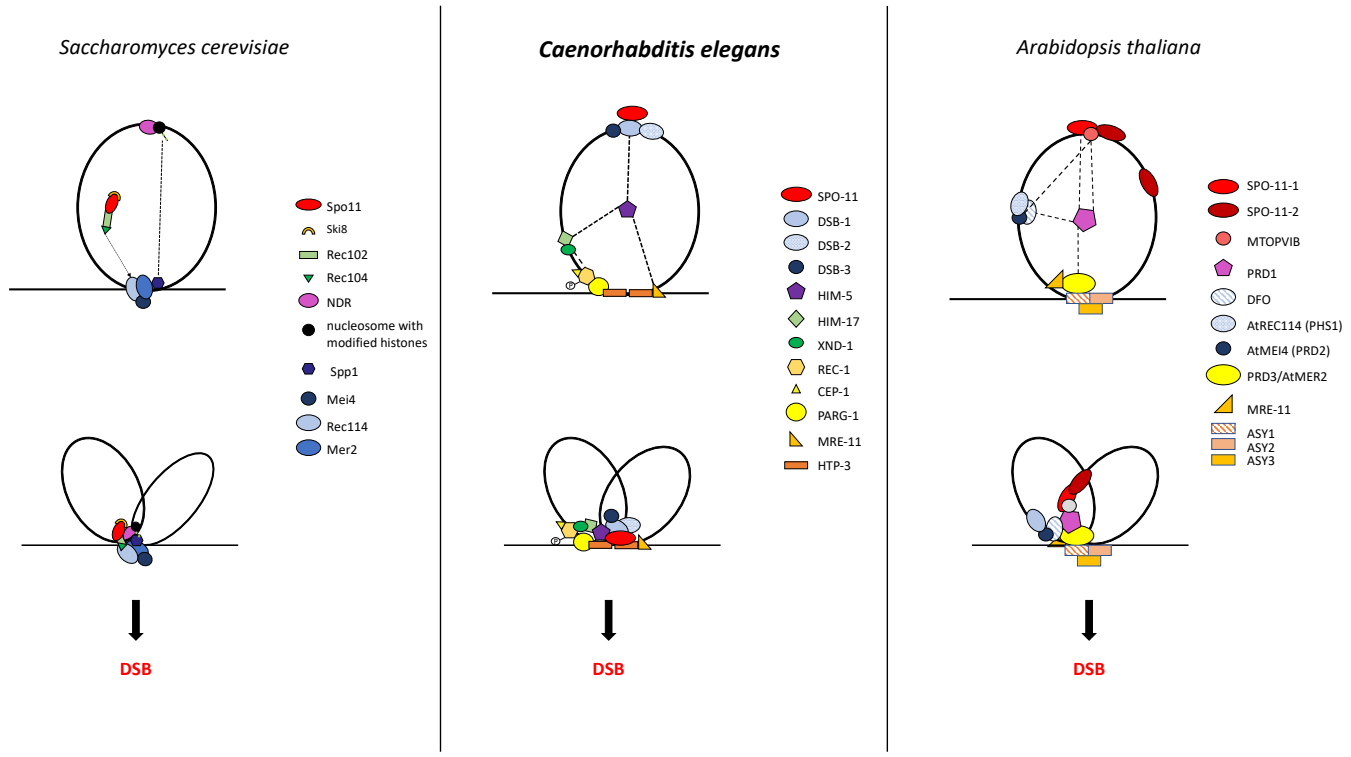

790 **Figure 4: Model of the DSB formation complex compared in *S. cerevisiae*, *C. elegans,***
791 **and *A. thaliana.*** The results of this paper and previous work discussed in this article allow us
792 to propose a model to explain the known interactions and localization patterns of the DSB
793 regulatory factors in *C. elegans* (center) where SPO-11 forms a subcomplex with DSB-1/-2/-3
794 that is located initially on the DNA loops and that we propose is brought to the chromosome
795 axes by association with HIM-5 and its binding to MRE-11 and PARG-1 which both associate
796 with HTP-3. SPO-11 could also be recruited to the DSB-1 after axis association. Other actors
797 of the complex are also initially on the chromatin loops and also get recruited to the axes by
798 HIM-5, allowing the formation of DSBs and coupling of DSBs to downstream repair by the MRN
799 complex and others. This model shares some similarities to what was proposed for *S.*
800 *cerevisiae* (Bouuaert et al., 2021b; Sommermeyer et al., 2013)and *A. thaliana* (Vrielynck et al.,
801 2021). For more details see the Discussion.

802

803 **SUPPLEMENTARY DATA**

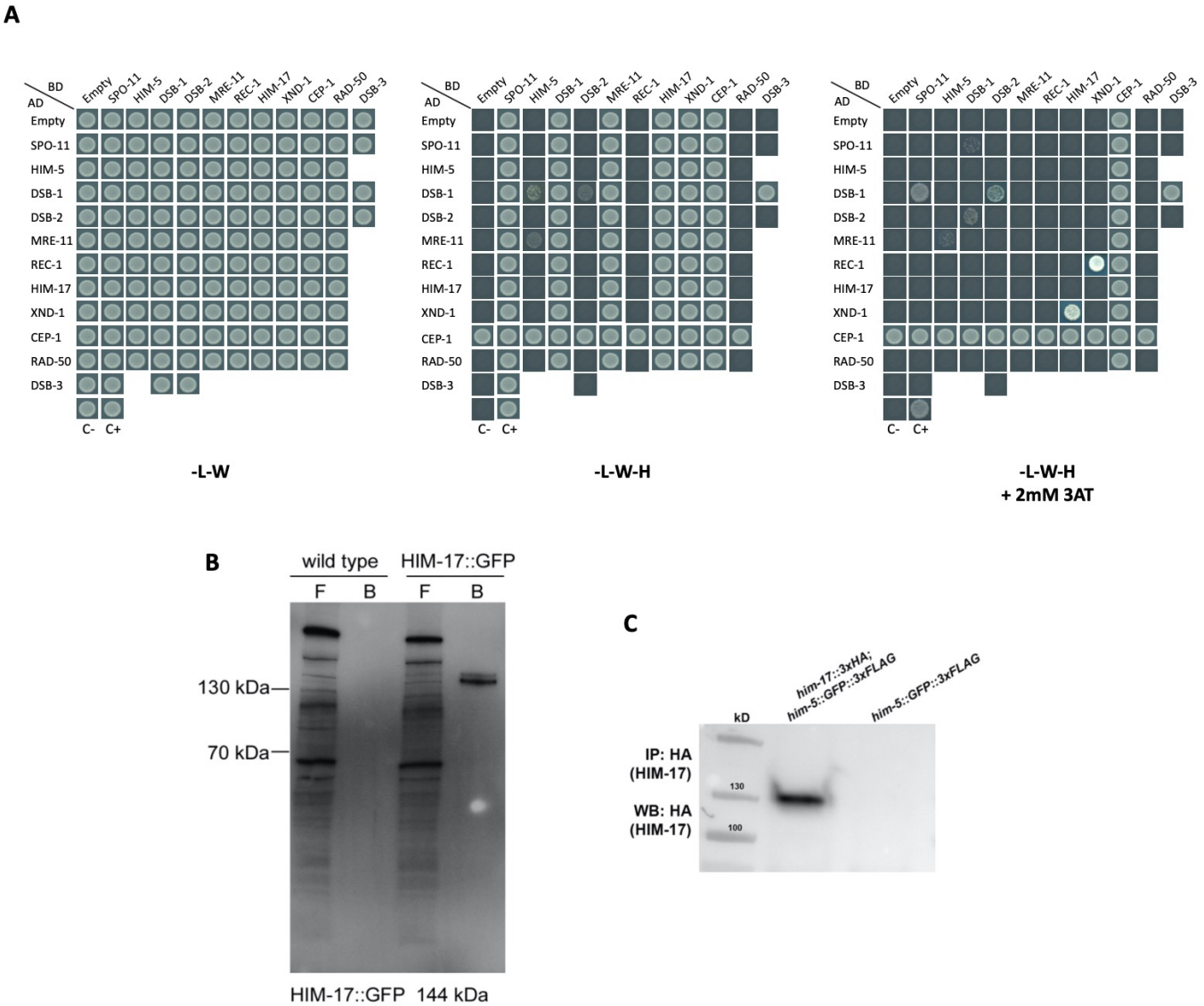

804
805
806 **Figure S1: Yeast-2-Hybrid studies and control IP data. A)** Representative Y2H
807 interactions between DSB factors, as monitored by growth in different media: (left) -L-W used
808 as a positive control; (center) -L-W-H showing weak interactions and, in some cases, self-
809 activation; (right) -L-W-H + 2mM 3AT (competitive inhibitor) showing strong interactions and
810 self-activation by CEP-1. Every DSB factor was tested here as activating domain (AD)
811 fusions as well as reciprocal DNA binding domain (BD) fusions. **B)** Western blot showing
812 immunoprecipitation of HIM-17 from *him-17::GFP* whole worm lysates using an anti-HIM-17
813 antibody. Unbound protein fraction (flow through, F) and proteins bound to the GFP trap
814 beads (B) from wild type and HIM-17::GFP transgenic worm lysates are shown. The HIM-
815 17::GFP-specific signal is enriched by using a GFP trap. **C)** Western blot showing
816 immunoprecipitation of HIM-17 from *him-17::3xHA;him-5::GFP::3xFLAG* whole worm lysates
817 using an anti-HIM-17 antibody.
818

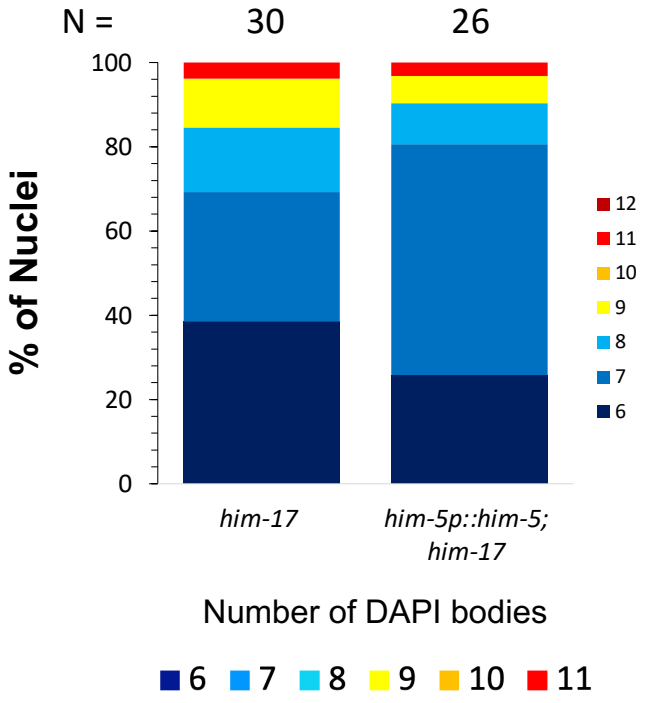

Figure S2 : Quantification of DAPI-stained bodies at diakinesis shows lack of rescue by HIM-5 expressed from its endogenous promoter. Colors correspond to the number of DAPI-stained bodies shown in the key below.

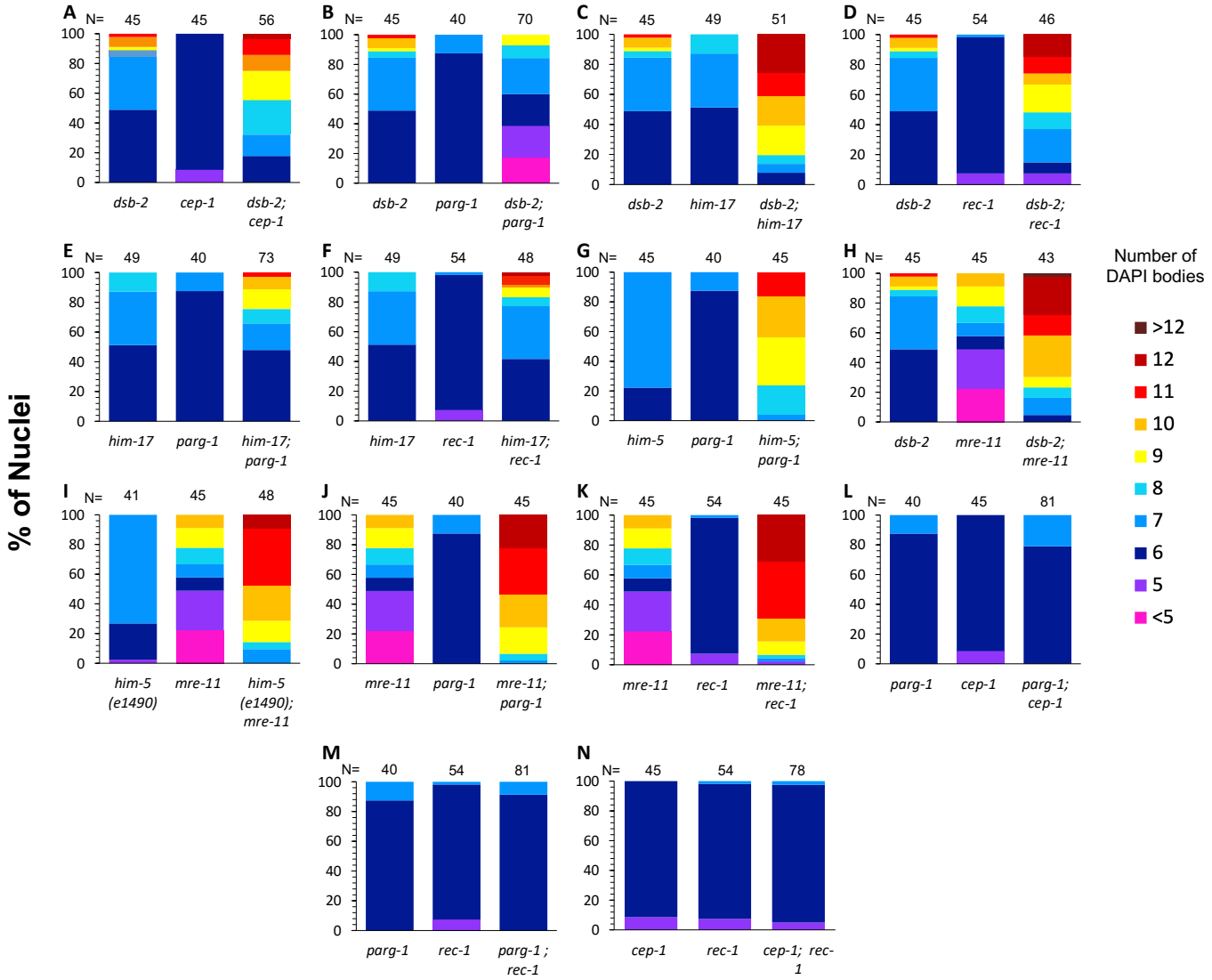

Figure S3: Epistasis analysis of DSB factors defines multiple genetic groups for crossover formation. **A-N)** Crossover formation is assessed by the number of DAPI-staining bodies at diakinesis**.** Each graph shows the quantification of DAPI-bodies in diakinesis nuclei for the indicated single and double mutants. Color indicates the number of DAPI-staining bodies. **O)** Genetic groups based on data presented here and previously published (Chung et al., 2015; Mateo et al., 2016; McClendon et al., 2016; Janisiw et al., 2020).

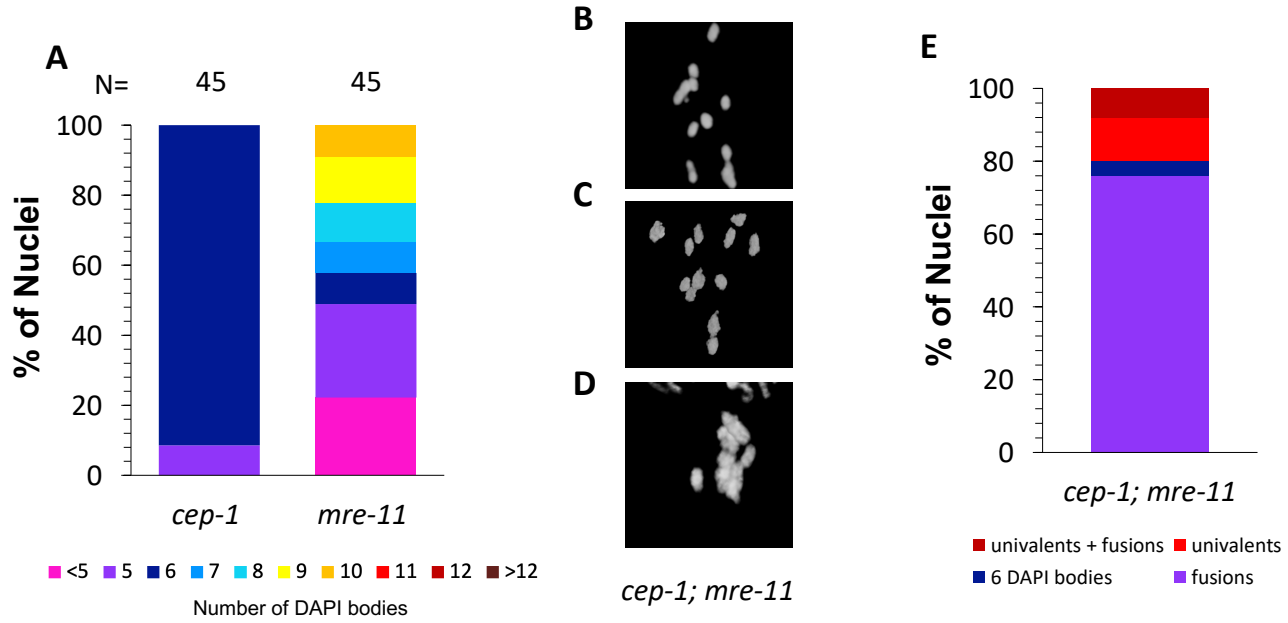

Figure S4: Mixed phenotypes are seen in *cep-1(lg12501;mre-11(iow1)* double mutants. A and E) Quantification of the number of DAPI-stained bodies at diakinesis for the indicated genotypes. Color indicates the number of DAPI-stained bodies**. B)** Representative DAPI-stained images of oocytes in diakinesis for *cep-1;mre-11* worms showing univalents (B, C) and fusions (D).

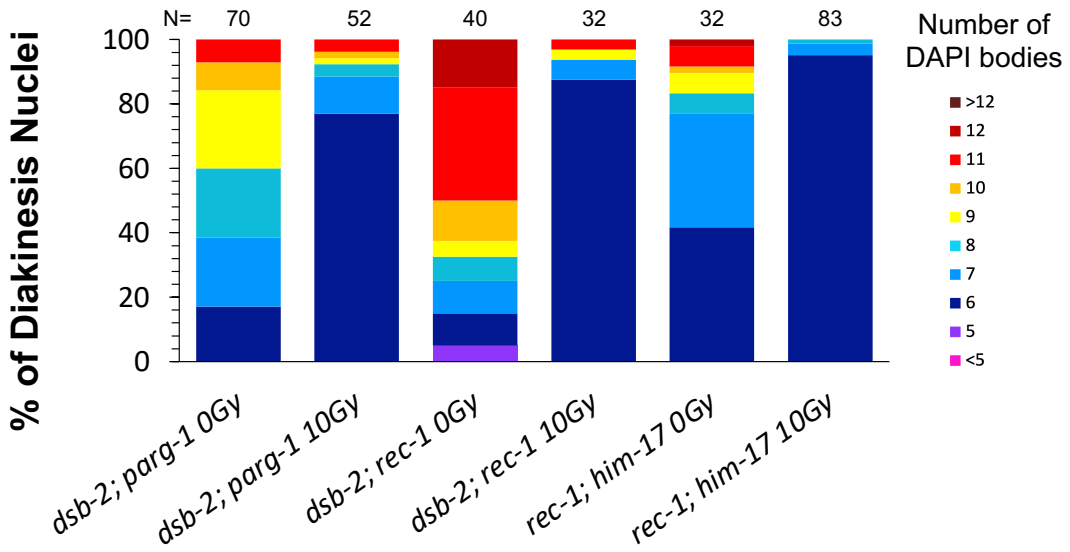

Figure S5: Irradiation rescues to crossover defects of assessory factor double mutant strains. Quantification of the number of DAPI-stained bodies at diakinesis for indicated genotypes with and without 10Gy of γ-irradiation. Color indicates the number of DAPI-staining bodies**.**

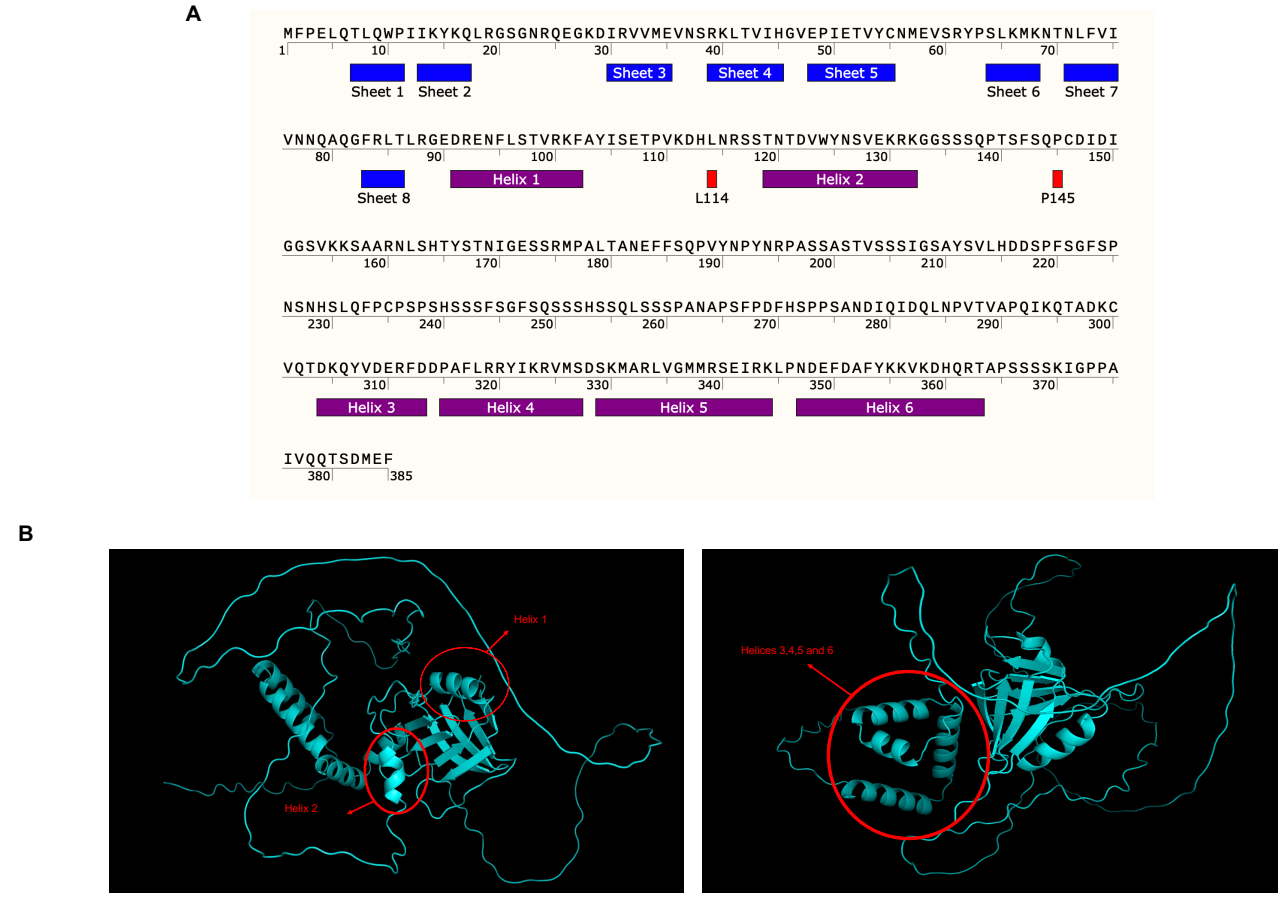

Figure S6: Putative structural analysis of DSB-1 identified potential interaction motifs. A) DSB-1 protein sequence. Secondary structures such as beta-sheets (blue) and alpha-helices (purple) are highlighted. In red are marked the sites where the deletions were introduced to create the truncated proteins used for yeast-two-hybrid in Figure 3. **B)** DSB-1 protein structure created by Alphafold2. Given that helixes are structures usually implicated in protein-protein interaction, some of them were deleted in the yeast-two-hybrid experiments shown in Figure 3. In this paper, we focused on the helix 2 and helices 3-6.

Strain	Genotype	Reference in text
N2	*C. elegans* var Bristol (N2).	Wild type
CA1117	*dsb-1(we11)* IV/*nT1[unc-?(n754) let-?]* (IV;V).	*dsb-1*
AV477	*dsb-2(me96)* II	*dsb-2*
RB1562	*him-5(ok1896)* V	*him-5(ok)*
CB4088	*him-5(e1490)* V	*him-5(e1490)*
CB6036	*him-17(e2806)* V	*him-17*
KR5305	*rec-1(h2875)* I	*rec-1*
VC130	*parg-1(gk120)* IV	*parg-1*
SSM2	*mre-11(iow1)/nT1[qIs51]* (IV;V)	*mre-11*
XY1054	*cep-1(lg12501)*	*cep-1*
QP1368	*rec-1(h2875)* I;*parg-1(gk120)* IV	*rec-1; parg-1*
QP1252	*rec-1(h2875);cep-1(lg12501)* I	*rec-1; cep-1*
QP1370	*cep-1(lg12501)* I;*parg-1(gk120)* IV	*parg-1; cep-1*
QP1317	*rec-1 (h2875)* I;*him-17(e2806)/nT1g* V	*rec-1; him-17*
QP1102	*rec-1(h2875)* I; *dsb-2(me96)* II	*dsb-2; rec-1*
QP 1367	*dsb-2(me96)* II;*parg-1(gk120)* IV	*dsb-2; parg-1*
QP1373	*dsb-2(me96)* II;*him-17(e2806)* V	*dsb-2; him-17*
QP1624	*dsb-2(me96)* II;*mre-11(iow1)/ unc-?(n754) let-?* (IV; V)	*dsb-2; mre-11*
QP1550	*cep-1(lg12501)* I;*dsb-2(me96)* II	*cep-1; dsb-2*
QP1573	*cep-1(lg12501)* I;*mre-11(iow1)/ nT1[qIs51]* (IV;V)	*cep-1; mre-11*
QP1366	*parg-1(gk120)* IV;*him-5(ok1896)* V	*him-5; parg-1*
QP1116	*mre-11(iow1), him-5(e1490)* V/ *nT1 [qIs51]* ((IV;V)	*him-5; mre-11*
QP1374	*parg-1(gk120)* IV; *him-17(e2806)* V	*him-17; parg-1*
QP1572	*parg-1(gk120)* IV;*mre-11(iow1)/nT1gU* [*unc-?(n754) let-?]* (IV; V)	*mre-11; parg-1*
QP1623	*rec-1(h2875)* I;*mre-11(iow1)/nT1gU [unc-?(n754) let-?]* (IV; V)	*mre-11; rec-1*
QP1907	*dsb-1(we11) IV/nT1 [qIs51]* (IV; V);*eaIs15[Ppie-1::him-5::gfp +unc-119(+)]*	*dsb-1/nT1; eaIs15*
QP1909	*dsb-2(me96)* II;*eaIs15[Ppie-1::him-5::gfp +unc-119(+)];*	*dsb-2; eaIs15*
QP1749	*him-17(ok424)* V;*eaIs15[Ppie-1::him-5::gfp + unc-119(+)];*	*eaIs15;him-17(ok424)*

QP1744	*him-17(ok424)* V;*eaIs4[Phim-5::him-5::gfp::3xFLAG + unc-119(+)]*	*eaIs4; him-17(ok424)*
PCM575	*dsb-1(icm97[GFP::dsb-1])* IV	*GFP::dsb-1*
NSV250	*him-5(ddr43[him-5::3XHA])*	*him-5::3xHA*
NSV205	*him-17(ddr37[him-17::3XHA])* V	*him-17::3xHA*
NSV508	*gfp::dsb-1;him-5::3xHA*	*GFP::dsb-1; him-5::3xHA*
QP??	*Phim-5*::*him-5*::*GFP*	*eaIs4*
NSV485	*eaIs4;him-17(ddr37[him-17::3XHA])* V	*him-17::3xHA; him-5::GFP::3xFLAG*
AV280	*unc-119(e2498) III; him-17(ok424) V; meIs5[unc-119(+) + him-17::GFP].*	*him-17::GFP*

Table S1: Strains and genetics. All strains were derived from the wild-type Bristol strain N2 and were cultivated at 20 °C under standard conditions. Abbreviated names and full genotypes of the strains used in this study are listed here.

Protein ID	Protein name/ORF	Predicted Molecular Weight (kD)	Sequence Coverage (%) Replicate 1	Replicate 2
CE13489	HIM-17	111.0 (954 aa)	38.7%	42.2%
CE51355	CKU-80	80.7 (713 aa)	1.4%	29.5%
CE28985	MSH-6	133.6 (1186 aa)	8%	12.3%
CE44308	CKU-70	77.9 (679 aa)	13.7%	15.2%
CE30653	RPC-2	129.1 (1154 aa)	7.1%	9.8%
CE42531	F33H1.4	156.5 (1378 aa)	3.6%	4.4%
CE26863	XND-1	78.3 (702 aa)	13.7%	7.4%
CE02015	CID-1	162.6 (1425 aa)	2.3%	5.5%
CE04148*	KLP-10	77.3 (690 aa)	3.6%	7.7%
CE28437	LSY-2	42.3 (365 aa)	10.10%	9.9%
CE41449	MEL-46	110.5 (973 aa)	2.4%	2.5%
CE27382	TAG-153	80.5 (733 aa)	8.7%	8.9%
CE01045	SNFC-5	42.8 (381 aa)	6.8%	6%
CE28922	F26F4.12	25.6 (231 aa)	10.8%	10.8%
CE16631	KLP-19	123.1 (1083 aa)	3.4%	2.1%
CE36164	LSL-1	36.9 (318 aa)	6.9%	7.2%

*Listed as pseudogene in WormBase version: WS288

Table S2: Immunoprecipitation (IP) from HIM-17::GFP whole worm extracts with an antibody against GFP analyzed by mass spectrometry. Sequence coverage refers to the percentage of the protein sequence that was pulled down in the HIM-17::GFP IP samples. Numbers are from two independent biological repeats.